1

Bulk and Surface Structure

We begin with some order of magnitude estimates and rules of thumb that will be justified in the remainder of this book. These estimates and rules introduce and underpin many of the most important concepts in surface science. The atom density in a solid surface is roughly $10^{15}\,\mathrm{cm}^{-2}$ ($10^{19}\,\mathrm{m}^{-2}$). The *Hertz-Knudsen equation*

$$Z_{\mathrm{w}} = \frac{p}{(2\pi m k_{\mathrm{B}} T)^{1/2}} \tag{1.0.1}$$

relates the *flux* of molecules striking a surface, Z_{w}, to the pressure (or equivalently the number density). Combining these two, we find that if the probability that a molecule stays on the surface after it strikes it (known as the *sticking coefficient s*) is unity, then it takes roughly 1 s for a surface to become covered with a film one molecule thick (a *monolayer*) when the pressure is 1×10^{-6} Torr. The process of molecules sticking to a surface is called *adsorption*. If we heat up the surface with a linear temperature ramp, the molecules will eventually leave the surface (desorb) in a well-defined thermal desorption peak and the rate of desorption at the top of this peak is roughly one monolayer per second. When molecules adsorb via chemical interactions, they tend to stick to well-defined sites on the surface. An essential difference between surface kinetics and kinetics in other phases is that we need to keep track of the number of empty sites. Creating new surface area is energetically costly and creates a region that is different from the bulk material. Size dependent effects lie at the root of nanoscience and two of the primary causes of size dependence are quantum confinement and when the influence of the surface becomes more important than that of the bulk.

We need to understand the structure of clean and adsorbate-covered surfaces and use this as a foundation for understanding surface chemical problems. We will use our knowledge of surface structure to develop a new strand of chemical intuition that will allow us to know when we can apply things that we have learned from reaction dynamics

Surface Science: Foundations of Catalysis and Nanoscience – Second Edition Kurt Kolasinski

in other phases and when we need to develop something completely different to understand reactivity in the adsorbed phase.

What do we mean by surface structure? There are two inseparable aspects to structure: *electronic structure* and *geometric structure*. The two aspects of structure are inherently coupled and we should never forget this point. Nonetheless, it is pedagogically helpful to separate these two aspects when we attack them experimentally and in the ways that we conceive of them.

When we speak of structure in surface science we can further subdivide the discussion into that of the clean surface, the surface in the presence of an adsorbate (*substrate structure*) and that of the adsorbate (*adsorbate structure* or *overlayer structure*). That is, we frequently refer to the structure of the first few layers of the substrate with and without an adsorbed layer on top of it. We can in addition speak of the structure of the adsorbed layer itself. Adsorbate structure not only refers to how the adsorbed molecules are bound with respect to the substrate atoms but also how they are bound with respect to one another.

1.1 Clean Surface Structure

1.1.1 Ideal Flat Surfaces

We are most concerned with transition metal and semiconductor surfaces. First we consider the type of surface we obtain by truncating the bulk structure of a perfect crystal. The most important crystallographic structures of metals are the face-centred cubic (fcc), body-centred cubic (bcc) and hexagonal close-packed (hcp) structures. Many transition metals of interest in catalysis take up fcc structures under normal conditions. Notable exceptions are Fe, Mo and W, which assume bcc structures and Co and Ru, which assume hcp structures. The most important structure for elemental (group IV: C, Si, Ge) semiconductors is the diamond lattice whereas compound semiconductors from groups III and V (III–V compounds, e.g. GaAs and InP) assume the related zincblende structure.

A perfect crystal can be cut along any arbitrary angle. The directions in a lattice are indicated by the *Miller indices*. Miller indices are related to the positions of the atoms in the lattice. Directions are uniquely defined by a set of three (fcc, bcc and diamond) or four (hcp) rational numbers and are denoted by enclosing these numbers in square brackets, e.g. [100]. hcp surfaces can also be defined by three unique indices and both notations are encountered as shown in Figure 1.3. A plane of atoms is uniquely defined by the direction that is normal to the plane. To distinguish a plane from a direction, a plane is denoted by enclosing the numbers associated with the defining direction in parentheses, e.g. (100). The set of all related planes with permutations of indices, e.g. (100), (010), (001), is denoted by curly brackets, such as {001}.

The most important planes to learn by heart are the *low index planes*. Low index planes can be thought of as the basic building blocks of surface structure as they represent some of the simplest and flattest of the fundamental planes. The low index planes in the fcc system, e.g. (100), (110) and (111), are shown in Figure 1.1. The low index planes of bcc symmetry are displayed in Figure 1.2 and the more complex structures of the hcp symmetry are shown in Figure 1.3

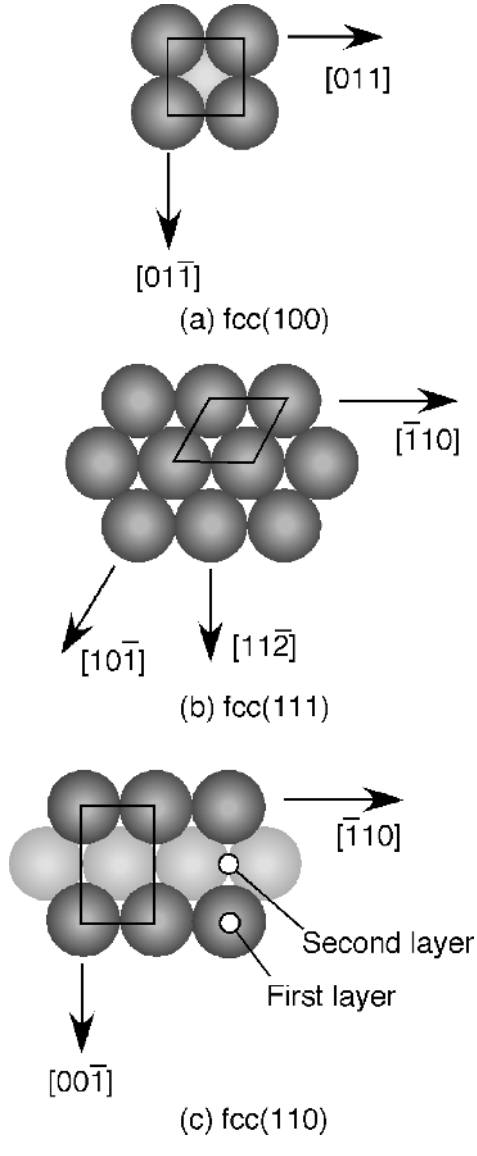

Figure 1.1 *Hard sphere representations of face-centred cubic (fcc) low index planes: (a) fcc (100); (b) fcc(111); (c) fcc(110).*

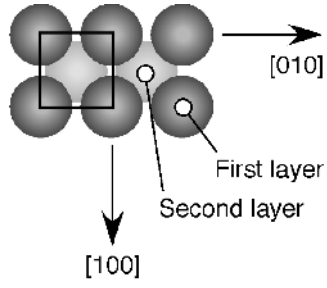

(a) bcc(100)

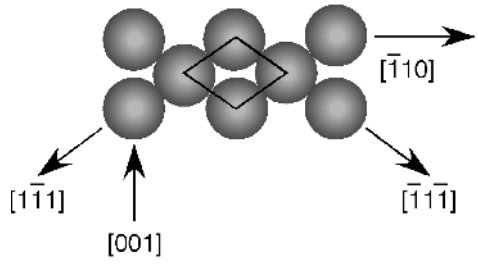

(b) bcc(110)

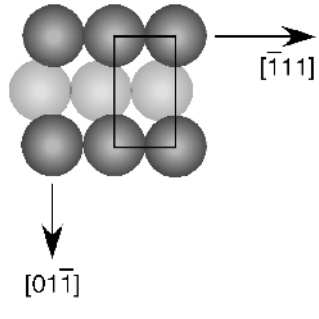

(c) bcc(211)

Figure 1.2 *Hard sphere representations of body-centred cubic (bcc) low index planes: (a) bcc(100); (b) bcc(110); (c) bcc(211).*

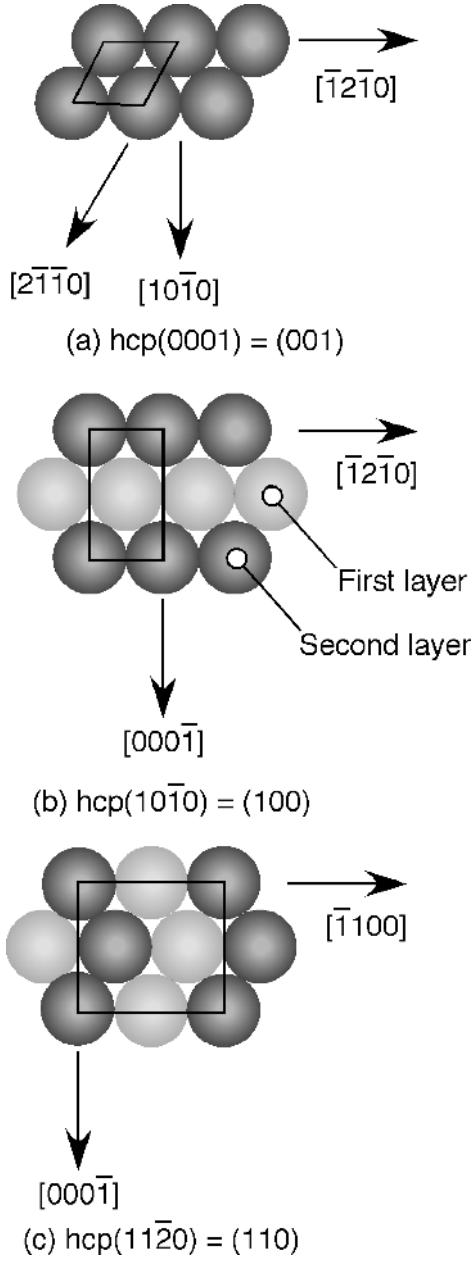

Figure 1.3 *Hard sphere representations of hexagonal close-packed (hcp) low index planes: (a) hcp(001) = (0001); (b) hcp($10\bar{1}0$) = hcp(100); (c) hcp($11\bar{2}0$) = hcp(110).*

We concentrate our discussion on Figure 1.1. The ideal structures shown in Figure 1.1 demonstrate several interesting properties. Note that these surfaces are not perfectly isotropic. We can pick out several *sites* on any of these surfaces that are geometrically unique. On the (100) surface we can identify sites of one-fold (on top of and at the centre of one atom), two-fold (bridging two atoms) or four-fold coordination (in the hollow between four atoms). The *coordination number* is equal to the number of surface atoms bound directly to the adsorbate. The (111) surface has one-fold, two-fold and three-fold coordinated sites. Among others, the (110) presents two different types of two-fold sites: a long bridge site between two atoms on adjacent rows and a short bridge site between two atoms in the same row. As one might expect based on the results of coordination chemistry, the multitude of sites on these surfaces leads to heterogeneity in the interactions of molecules with the surfaces. This will be important in our discussion of adsorbate structure as well as for surface chemistry.

A very useful number to know is the *surface atom density*, σ_0. Nicholas[1] has shown that there is a simple relationship between σ_0 and the Miller indices *hkl*,

$$\sigma_0 = \frac{1}{A_{hkl}} = \frac{4}{Qa^2(h^2+k^2+l^2)^{1/2}} \text{ for fcc and bcc} \tag{1.1.1}$$

$$\text{and} \qquad \sigma_0 = \frac{1}{A_{hkl}} = \frac{2}{a^2[4r^2(h^2+hk+k^2)+3l^2]^{1/2}} \text{ for hcp.} \tag{1.1.2}$$

In these expressions, A_{hkl} is the area of the *surface unit cell*, a is the bulk lattice parameter, r is the hcp axial ratio given in Table 1.1 and Q is defined by the following rules:

$$\text{bcc} : Q = 2 \text{ if } (h+k+l) \text{ is even}, Q = 4 \text{ if} (h+k+l) \text{ is odd}$$
$$\text{fcc} : Q = 1 \text{ if } h, k, \text{and } l \text{ are all odd, otherwise } Q = 2.$$

Table 1.1 lists the surface atoms densities for a number of transition metals and other materials. The surface atom density is highest for the (111) plane of an fcc crystal, the (100) plane for a bcc crystal, and an (0001) plane for an hcp crystal. A simple constant factor relates the atom density of all other planes within a crystal type to the atom density of the densest plane. Therefore, the atom density of the (111) plane along with the relative packing factor is listed for the fcc, bcc and hcp crystal types.

The formation of a surface from a bulk crystal is a stressful event. Bonds must be broken and the surface atoms no longer have their full complement of coordination partners. Therefore, the surface atoms find themselves in a higher energy configuration compared with being buried in the bulk and they must relax. Even on flat surfaces, such as the low index planes, the top layers of a crystal react to the formation of a surface by changes in their bonding geometry. For flat surfaces, the changes in bond lengths and bond angles usually only amount to a few percent. These changes are known as *relaxations*. Relaxations can extend several layers into the bulk. The near surface region, which has a structure different from that of the bulk, is called the *selvage*. This is our first indication that bonding at surfaces is inherently different from that in the bulk both because of changes in coordination and because of changes in structure. On metal surfaces, the force (*stress*) experienced by surface atoms leads to a contraction of the interatomic distances in the surface layer.

Table 1.1 *Surface atom densities. Data taken from Roberts and Mckee[2] except where noted.*

fcc structure							
Plane	(100)	(110)	(111)	(210)	(211)	(221)	
Density relative to (111)	0.866	0.612	1.000	0.387	0.354	0.289	
Metal	Al	Rh	Ir	Ni	Pd	Pt	Cu
Density of (111)/cm^{-2} $\times 10^{-15}$	1.415	1.599	1.574	1.864	1.534	1.503	1.772
Metal	Ag	Au					
Density of (111)/cm^{-2} $\times 10^{-15}$	1.387	1.394					
bcc structure							
Plane	(100)	(110)	(111)	(210)	(211)	(221)	
Density relative to (110)	0.707	1.000	0.409	0.316	0.578	0.236	
Metal	V	Nb	Ta	Cr	Mo	W	Fe
Density of (100)/cm^{-2} $\times 10^{-15}$	1.547	1.303	1.299	1.693	1.434	1.416	1.729
hcp structure							
Plane	(0001)	$(10\bar{1}0)$	$(10\bar{1}1)$	$(10\bar{1}2)$	$(11\bar{2}2)$	$(11\bar{2}2)$	
Density relative to (0001)	1.000	$\frac{3}{2r}$	$\frac{\sqrt{3}}{(4r^2+3)^{1/2}}$	$\frac{\sqrt{3}}{(4r^2+12)^{1/2}}$	$\frac{1}{r}$	$\frac{1}{2(r^2+1)^{1/2}}$	
Metal	Zr	Hf	Re	Ru	Os	Co	Zn
Density of (0001)/cm^{-2} $\times 10^{-15}$	1.110	1.130	1.514	1.582	1.546	1.830	1.630
Axial ratio $r = c/a$	1.59	1.59	1.61	1.58	1.58	1.62	1.86
Metal	Cd						
Density of (0001)/cm^{-2} $\times 10^{-15}$	1.308						
Axial ratio $r = c/a$	1.89						
	Diamond lattice					Graphite	
Element	C	Si (111)	Ge			C	
Areal Density/cm^{-2} $\times 10^{-15}$		0.7839 (100) 0.6782	(100) 0.625			basal plane 3.845	

Si values[3]

1.1.2 High Index and Vicinal Planes

Surface structure can be made more complex either by cutting a crystal along a higher index plane or by the introduction of *defects*. *High index planes* (surfaces with h, k, or $l > 1$) often have open structures that can expose second and even third layer atoms. The fcc(110) surface shows how this can occur even for a low index plane. High index planes often have large unit cells that encompass many surface atoms. An assortment of defects is shown in Figure 1.4.

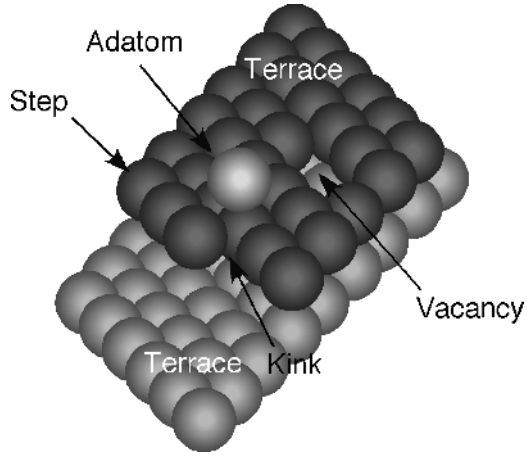

Figure 1.4 *Hard-sphere representation of a variety of defect structures that can occur on single-crystal surfaces.*

One of the most straightforward types of defects at surfaces is that introduced by cutting the crystal at an angle slightly off the perfect [*hkl*] direction. A small miscut angle leads to *vicinal surfaces*. Vicinal surfaces are close to but not flat low index planes. The effect of a small miscut angle is demonstrated in Figure 1.4. Because of the small miscut angle, the surface cannot maintain the perfect (*hkl*) structure over long distances. Atoms must come in whole units and in order to stay as close to a low index structure as possible while still maintaining the macroscopic surface orientation, step-like discontinuities are introduced into the surface structure. On the microscopic scale, a vicinal surface is composed of a series of *terraces* and *steps*. Therefore, vicinal surfaces are also known as *stepped surfaces*.

Stepped surfaces have an additional type of heterogeneity compared with flat surface, which has a direct effect on their properties[4]. They are composed of terraces of low index planes with the same types of symmetry as normal low index planes. In addition, they have steps. The structure of step atoms must be different from that of terrace atoms because of the different bonding that they exhibit. Step atoms generally relax more than terrace atoms. The effect of steps on electronic structure is illustrated in Figure 1.5. The electrons of the solid react to the presence of the step and attempt to minimize the energy of the defect. They do this by spreading out in a way that makes the discontinuity at the step less abrupt. This process is known as *Smoluchowski smoothing*.[5] Since the electronic structure of steps differs from that of terraces, we expect that their chemical reactivity is different as well. Note that the top and the bottom of a step are different and this has implications, for

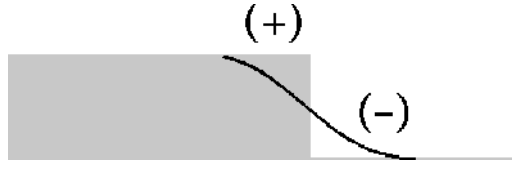

Figure 1.5 *Smoluchowski smoothing: the electrons at a step attempt to smoothe out the discontinuity of the step.*

instance, for diffusion of adsorbates over steps. It is often the case that diffusion in one direction is significantly easier than in the other. Furthermore, we expect that diffusion on the terraces may differ significantly from diffusion across steps (Section 3.2).

1.1.3 Faceted Surfaces

Not all surfaces are stable. The formation of a surface is always endothermic (see Ch. 5). However, the formation of a larger surface area of low energy (low index) planes is sometimes favoured over the formation of a single layer of a high-energy (high index) plane. Many high index planes are known to *facet* at equilibrium. Faceting is the spontaneous formation of arrays of low index planes. Numerous systems exhibit ordered arrays of low index facets. These have been catalogued by Shchukin and Bimberg[6] and include vicinal surfaces of Si(111), GaAs(100), Pt(100), high index planes of Si(211) and low index planes of TaC(110).

1.1.4 Bimetallic Surfaces

A surface composed of a mixture of two metals often exhibits unique properties. The catalytic behaviour of Au+Ni surfaces, for example, will be discussed in Chapter 6. The surface *alloy* of $Pt_3Sn(111)$ has also attracted interest because of its unusual catalytic properties.[7] Materials containing mixtures of metals introduce several new twists into a discussion of surface structure. Here it is important to make a distinction between an alloy, that is a solid solution of one metal randomly dissolved in another, and an *intermetallic compound*, that is, a mixture with a definite and uniform stoichiometry and unit cell. Consider a single crystal composed of two metals that form a true intermetallic compound. An ideal single crystal sample would exhibit a surface structure much like that of a monometallic single crystal. The composition of the surface would depend on the bulk composition and the exposed surface plane. Several examples of this type have been observed,[8], e.g. $Cu_3Au(100)$; (100), (111) and (110) surfaces of Ni_3Al; (110) and (111) surfaces of NiAl as well as $TiPt_3(100)$.

Not all combinations of metals form intermetallic compounds. Some metals have limited solubility in other metals. In a *solid solution*, just as for liquid solutions, the solute will tend to be randomly distributed in the solvent. Furthermore, the solubility of a given metal may be different in the bulk than it is at the surface. That is, if the surface energy of one component of an alloy is significantly lower than that of the other component, the low surface energy species preferentially segregates to the surface. This leads to enrichment in the surface concentration as compared with the bulk concentration. Most alloys show some degree of segregation and enrichment of one component at the surface or in subsurface sites. The factors that lead to segregation are much the same as those that we will encounter in Chapter 7 when we investigate growth processes. For a binary alloy AB, the relative strengths of the A–A, A–B and B–B interactions as well as the relative sizes of A and B determine whether alloy formation is exothermic or endothermic. These relative values determine whether segregation occurs. If alloy formation is strongly exothermic, i.e. the A–B interaction is stronger than either A–A or B–B interactions, then there is little tendency toward segregation. The relative atomic sizes are important for determining whether lattice strain influences the energetics of segregation. In summary, surface segregation is expected unless alloy formation is highly exothermic and there is good matching of the atomic radii.

If a bimetallic surface is made not from a bulk sample but instead from the deposition of one metal on top of another, the surface structure depends sensitively on the conditions under which deposition occurs. In particular, the structure depends on whether the deposition process is kinetically or thermodynamically controlled. These issues will be dealt with in Chapter 7.

From these considerations, we can conceive of at least four configurations that arise from the deposition of one metal on top of another, as shown in Figure 1.6. The formation of an intermetallic compound with a definite composition is illustrated in Figure 1.6(a). The surface is rather uniform and behaves much as a pure metal surface with properties that are characteristic of the alloy and in all likelihood intermediate between the properties of either one of the constituent pure metals. If one metal is miscible in the other, it can incorporate itself into the surface after deposition. A random array of incorporated atoms [Figure 1.6(b)] is expected to dope the substrate. Doping means that the added atom changes the electronic character of the substrate metal. Thereby, the chemical reactivity and other properties, such as magnetism or work function, may also change. Whether the doping effect is long range or short range is greatly debated. An immiscible metal segregates into structures that minimize the surface area. Often step edges present sites with a high binding energy, which can lead to the structure shown in Figure 1.6(c). If the binding of adatoms to themselves is stronger than to the substrate atoms, we expect the formation of islands to occur as shown in Figure 1.6(d). In Chapter 6 we will explore the implications of these different structures on catalytic reactivity.

1.1.5 Porous Solids

It is standard usage to refer to a solid substance by adding a suffix to its chemical notation to denote its phase. Hence crystalline Si is c-Si, amorphous Si is a-Si, alumina in the β structure is β-Al_2O_3 and in the gamma structure γ-Al_2O_3. In this same convention I will denote a nanocrystalline substance as, for example, nc-Si and a porous solid, for example, por-Si. This general notation avoids several possible ambiguities compared with some notation that is used in the literature. For instance, p-Si or pSi is sometimes used for porous silicon but also sometimes for *p*-doped Si.

A number of parameters are used to characterized *porous solids*. They are classified according to their mean pore size, which for a circular pore is measured by the pore diameter. The International Union of Pure and Applied Chemistry (IUPAC) recommendations define samples with a mean pore size < 10 nm as microporous, between 10 and 100 nm as mesoporous, and > 100 nm as macroporous. The term nanoporous is currently in vogue but undefined. The *porosity* ε is a measure of the relative amount of empty space in the material,

$$\varepsilon = V_{\mathrm{p}}/V, \tag{1.1.3}$$

where V_{p} is the pore volume and V is the apparent volume occupied the material. We need to distinguish between the *exterior surface* and the *interior surface* of the material. If we think of a thin porous film on top of a substrate, the exterior surface is the upper surface of the film (taking into account any and all roughness), whereas the interior surface comprises the surface of all the pore walls that extend into the interior of the film.

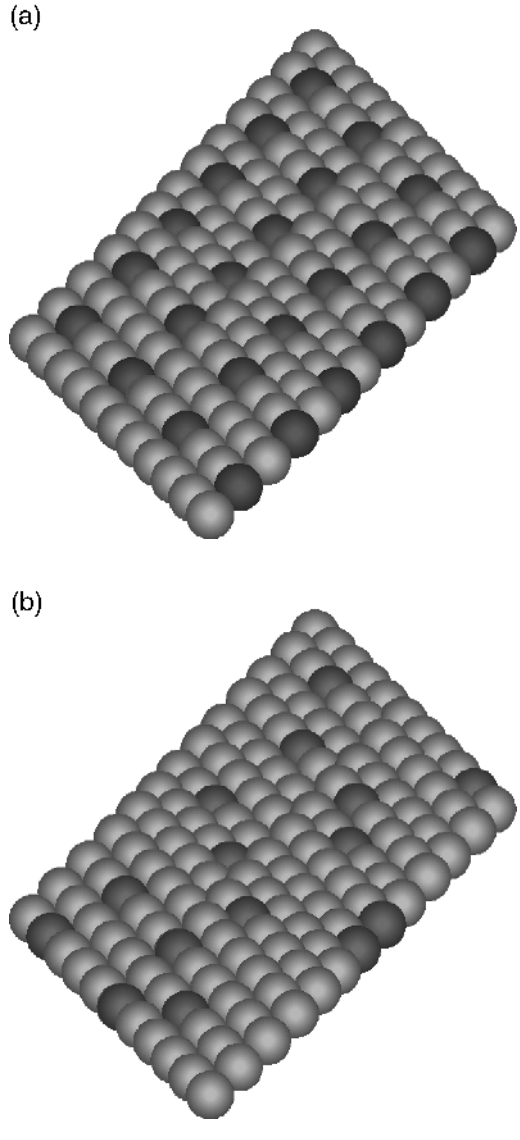

Figure 1.6 *Four limiting cases of the structure of a bimetallic surface prepared by metal-on-metal adsorption: (a) the formation of an intermetallic compound with a definite stoichiometry; (b) random absorption of a miscible metal; (c) segregation of an immiscible metal to the step edges; (d) segregation of an immiscible metal into islands.*

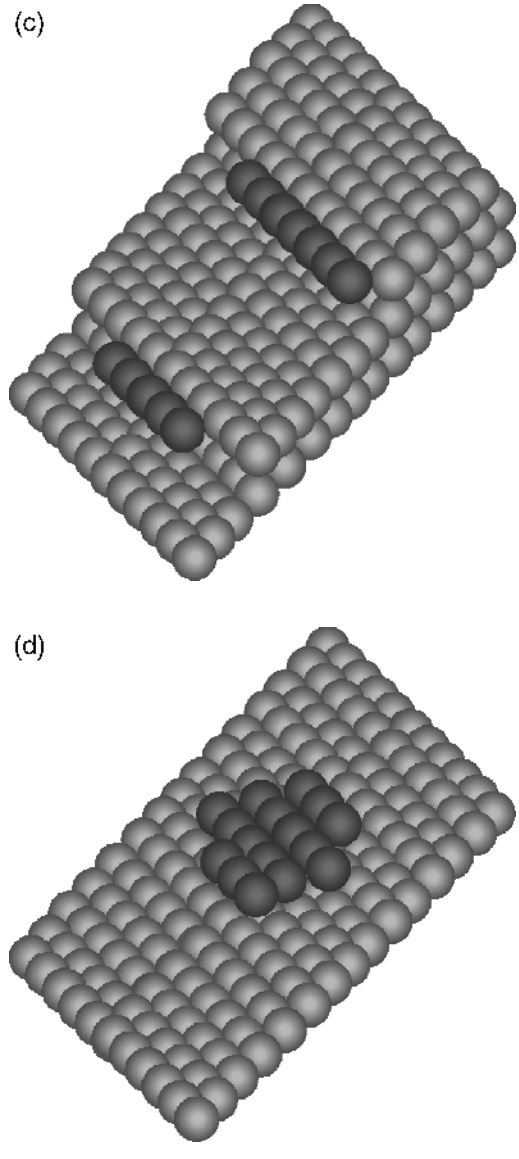

Figure 1.6 *(Continued)*

The *specific area* of a porous material, a_p, is the accessible area of the solid (the sum of exterior and interior areas) per unit mass.

Porous solids can be produced in several ways. They can be grown from a molecular beam incident at a high angle in a technique known as *glancing angle deposition* (GLAD).[9] Porous solids are often produced by etching an originally nonporous solid, for instance Si,[10] Ge, SiC, GaAs, InP, GaP and GaN[11] as well as Ta_2O_5,[12] TiO_2,[13] WO_3,[14] ZrO_2[15] and Al_2O_3.[16] Mesoporous silicas and transition metal oxides (also called

molecular sieves) are extremely versatile and can exhibit pore sizes from 2–50 nm and specific areas up to $1500\,m^2\,g^{-1}$. They can be synthesized using a *liquid crystal templating* method that allows for control over the pore size.[17, 18] A similar templating strategy has also been used to produce mesoporous Ge[19] and porous Au.[20] By using a template of latex or silica microspheres (or more generally colloidal crystals), this range can be extended into the macroporous regime for a broad range of materials, including inorganic oxides, polymers, metals, carbon and semiconductors.[21] This method involves creating a mixture of the template and the target material. The template *self-assembles* into a regular structure and the target fills the space around the template. Subsequently the template is removed by combustion, etching, some other chemical reaction or dissolution leaving behind the target material in, generally, a powder of the porous material.

Porous materials are extremely interesting for the optical, electronic and magnetic properties[10, 22] as well as membranes.[23, 24] A much more in depth discussion of their use in catalysis can be found in Thomas and Thomas.[25] Porous oxides such as Al_2O_3, SiO_2 and MgO are commonly used as (relatively) inert, high surface areas substrates into which metal clusters are inserted for use as heterogeneous catalysts. These materials feature large pores so that reactants can easily access the catalyst particles and products can easily leave them. *Zeolites* are microporous (and more recently mesoporous) aluminosilicates, aluminium phosphates (ALPO), metal aluminium phosphates (MeALPO) and silicon aluminium phosphates (SAPO) that are used in catalysis, particularly in the refining and reforming of hydrocarbons and petrochemicals. Other atoms can be substituted into the cages and channels of zeolites, enhancing their chemical versatility. Zeolites can exhibit both acidic and basic sites on their surfaces that can participate in surface chemistry. Microporous zeolites constrain the flow of large molecules; therefore, they can be used for *shape-selective catalysis*. In other words, only certain molecules can pass through them so only certain molecules can act as reactants or leave as products.

Another class of microporous materials with porous smaller than 2 nm is that of *metal-organic frameworks* (MOF).[26–28] MOFs are crystalline solids that are assembled by the connection of metal ions or clusters through molecular bridges. Control over the void space between the metal clusters is easily obtained by controlling the size of the molecular bridges that link them. Implementation of a strategy that incorporates the geometric requirements for a target framework and transforms starting materials into such a framework has been termed *reticular synthesis*. As synthesized MOFs generally have their pores filled with solvent molecules because they are synthesized by techniques common to solution phase organic chemistry. However, the solvent molecules can generally be removed to expose free pores. Closely related are covalent organic frameworks (COF) which are composed entirely of light elements including H, B, C, N and O.[29]

1.1.6 Oxide Surfaces

Oxides are covalent solids that exhibit a range of interesting properties. Most oxides can assume a number of structural forms. Metals often have more than one oxidation state, which means that they are able to form oxides of different stoichiometries or even mixed valence compounds in which more than valence state is present. Different crystal

structures have different optical and electronic properties. Defects as well as substitutional or interstitial impurities (dopants) also modify the optical and electronic properties as well as the chemistry of oxides. Because of the multifarious crystal structures exhibited by oxides, it is more difficult to present general patterns in structure and reactivity.[30]

Many oxides are insulators with band gaps in excess of 6 eV, such as SiO_2 (silica, quartz, glass, 35 different crystalline forms), Al_2O_3 (alumina, corundum or α-alumina as well as γ-alumina, which has a defect spinel structure, and several others) and MgO (magnesia with a NaCl structure). All of these are commonly used as substrates for supported catalysts. γ-alumina is particularly important for catalysis and it is found that it can take up water into its structure.[31] The H content in γ-alumina may fall anywhere within the range $[0 < n < 0.6]$ for $Al_2O_3 \cdot n(H_2O)$. α-alumina doped with metal impurities is responsible for sapphire (Cr, Fe, or Ti doped) and ruby (Cr doped).

Other oxides are conductors or at least semiconductors with bandgaps below 4 eV such as cerium oxides (ceria, CeO_2 with a fluorite structure but also Ce_2O_3), In_2O_3 (bixbyite type cubic structure and an indirect bandgap of just 0.9–1.1 eV), SnO_2 (rutile, 3.6 eV direct bandgap) and ZnO (wurzite, 3.37 eV direct bandgap). The ability of ceria to form two different valence states allows its surface and near surface region to exist in a range of stoichiometries between CeO_2 and Ce_2O_3. As we shall see later, when used as an additive to the catalyst support for automotive catalysis, this allows ceria to act as a sponge that takes up or gives off oxygen atoms based on the reactive conditions. By substituting approximately 10 % Sn into indium oxide, the resulting material indium tin oxide (ITO) combines two seemingly mutually exclusive properties: a thin film of ITO is both transparent and electrically conductive. This makes ITO very important as a substrate in display technology. The properties of semiconducting oxides are responsive not only to oxygen content and metal atom substitution. Because they are semiconductors, their electrical and optical properties are also strongly size dependent when formed into nanotubes, nanowires and nanoparticles due to the effects of quantum confinement.

The covalent nature of oxides means that certain *cleavage planes* are much more favoured to form surfaces, that is, there are certain low energy planes that are much more stable and likely to be observed. This is in contrast to metals. Metallic bonding is much less directional and this means that several planes have similar surface energies and it is easier to make samples of crystalline metals that exhibit a variety of different planes. Another consequence of directional bonding is that the surfaces of covalent solids are much more susceptible to reconstruction.

The stability of covalent surfaces is described by *Tasker's rules*.[32] The surfaces of ionic or partly ionic crystals can be classified according to three types, as shown in Figure 1.7. Type 1 consists of neutral planes containing a counterbalancing stoichiometry of anions and cations. Type 2 is made up of symmetrically arranged layers of positive and negative charged, which when taken as a repeat unit contain no net charge and no net dipole moment perpendicular to the unit cell. Type 3 exhibits a surface charge and there is a dipole moment perpendicular to the unit cell. Types 1 and 2 represent stable surfaces that exhibit a good balance of charge at the surface. Polar surfaces of Type 3 have very large surface energies would be unstable. These surfaces cannot exist unless they are stabilized by extensive reconstruction, faceting or the adsorption of counterbalancing charge.

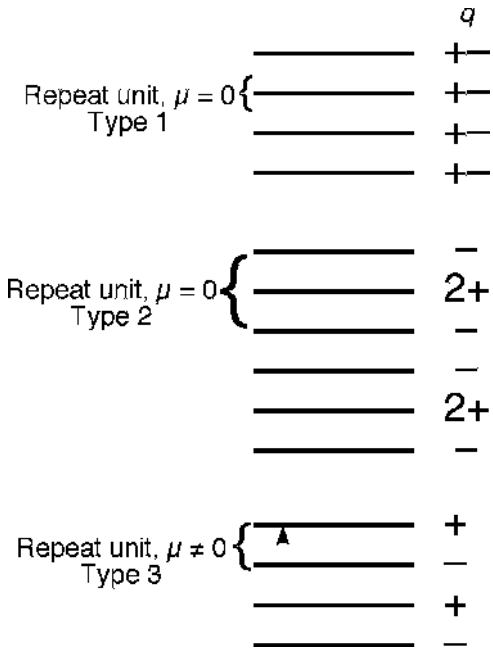

Figure 1.7 *Three types of planes formed by ionic crystals. q, ionic charge in layer; μ electric dipole moment associated with the lattice repeat unit.*

The rocksalt (NaCl) structure is common among binary oxides of the general formula MX such as MgO and NiO. Both the (100) and (110) are stoichiometric planes of Type 1 with equal numbers of m^+ and X^- ions. Both are low energy planes and the {100} planes are the natural cleavage planes for rocksalt crystals. The (111) plane is of Type 3 and, therefore, is only expected to be observed in a bulk crystal if stabilized by reconstruction or adsorption, though it might be observed in a potentially metastable thin film.

The fluorite structure is common for MX_2 oxides such as CeO_2. Here the (100) is a Type 3 plane. While the (110) is a Type 1 plane, the (111) plane with exposed O^{2-} anions at its surface is of Type 2, has the lowest energy, and is the natural cleavage plane of a fluorite crystal. A (111) plane that is terminated by metal cations is of Type 3 and is not normally observed.

The zincblende structure is characteristic of compound semiconductors such as GaAs and ZnS. While not oxides they are partially ionic. The (110) plane is the natural cleavage plane as it is neutral and of Type 1. Both the (100) and (111) are Type 3 planes and are unstable with respect to reconstruction.

One way to avoid the difficulties of working with bulk oxide crystals is to grow thin films of oxides on top of metal single crystals[33] with the techniques described in Chapter 7. With this approach a range of materials can then be probed using the techniques of surface science to probe structure and reactivity.

An oxide of particular interest is that of TiO_2, titania.[34,35] The two most important crystalline forms of titania are rutile and anatase. Rutile has a bandgap of ~3.2 eV, which means that it absorbs in the near UV by excitation from filled valence band states

localized essentially on an O(2*p*) orbital to the empty conduction band states primarily composed of Ti(3*d*) states. Such excitations lead to very interesting photocatalytic properties. The (110) plane is the most stable and it can assume several different *reconstructions* as shown in Figure 1.8. The different reconstructions occur in response to the oxygen content of the crystal. The release of oxygen caused by heating the sample in a vacuum drastically changes the optical properties, changing a perfectly stoichiometric TiO_2 from transparent to blue to black with progressive loss of O atoms. A substoichiometric oxide TiO_{2-x} will turn black for value of $x = 0.01$.

As Figure 1.8(a) shows, the expected (1×1) structure is found on stoichiometric TiO_2 and for surfaces for which x is very small (corresponding to blue crystals). The images are dominated by five-fold coordinate Ti atoms in the surface. Oxygen ions are not usually imaged by STM and the reasons why different atoms image differently will be discussed in Chapter 2, as is the $(n\times m)$ nomenclature that indicate the size of the reconstruction unit cell compared with the unreconstructed (1×1) unit cell. As the crystal loses more O atoms changes occur, as shown in Figure 1.8 (a)–(d). The structure first changes to a (1×3) pattern, which only exists over only a narrow range of x. This is followed by two different (1×2) reconstructions. The first is an added row reconstruction. The second (1×2) structure is really an $(n\times2)$ where n is a large, but variable number for any particular surface (that is, the structure often lacks good order in the [001] direction).

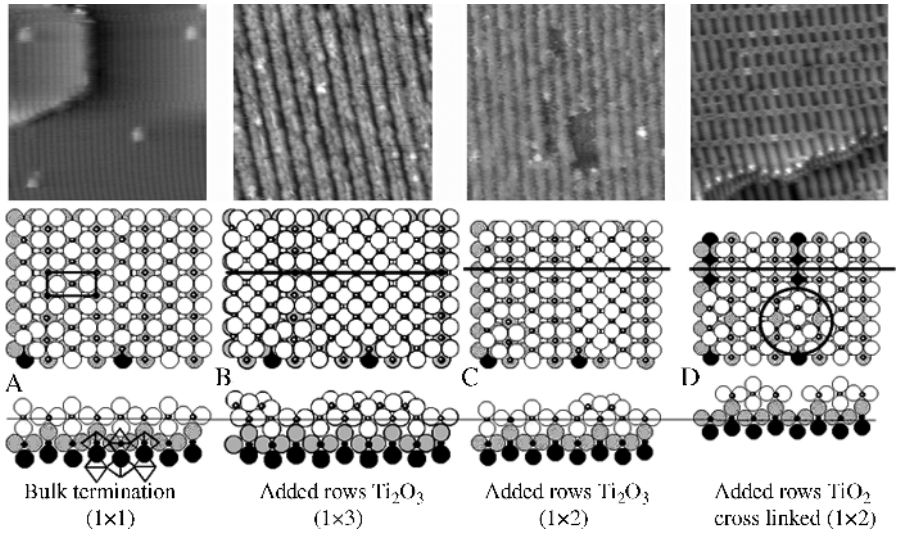

Figure 1.8 *The surface structures observed on TiO_2(110) as a function of increasing bulk reduction of the crystal. Upper panels are scanning tunnelling microscope images with 20 nm scan size. The lower two panels display the proposed surface structures. Reproduced from M. Bowker, Curr. Opin. Solid State Mater. Sci.* **10**, *153. Copyright (2006), with permission from Elsevier Science.*

1.2 Reconstruction and Adsorbate Structure

1.2.1 Implications of Surface Heterogeneity for Adsorbates

As we have alluded to above, the natural heterogeneity of solid surfaces has several important ramifications for adsorbates. Simply looked at from the point of view of electron density, we see that low index planes, let alone vicinal surfaces, are not completely flat. Undulations in the surface electron density exist that reflect the symmetry of the surface atom arrangement as well as the presence of defects such as steps, missing atoms or impurities. The ability of different regions of the surface to exchange electrons with adsorbates, and thereby form chemical bonds, is strongly influenced by the coordination number of the various sites on the surface. More fundamentally, the ability of various surface sites to enter into bonding is related to the symmetry, nature and energy of the electronic states found at these *sites*. It is a poor approximation to think of the surface atoms of transition metals as having unsaturated valences (dangling bonds) waiting to interact with adsorbates. The electronic states at transition metal surfaces are extended, delocalized states that correlate poorly with unoccupied or partially occupied orbitals centred on a single metal atom. The concept of dangling bonds, however, is highly appropriate for covalent solids such as semiconductors. Nontransition metals, such as aluminium, can also exhibit highly localized surface electronic states.

The heterogeneity of low index planes presents an adsorbate with a more or less regular array of sites. Similarly, the strength of the interaction varies in a more or less regular fashion that is related to the underlying periodicity of the surface atoms and the electronic states associated with them. These undulations are known as *corrugation*. Corrugation can refer to either geometric or electronic structure. A corrugation of zero corresponds to a completely flat surface. A high corrugation corresponds to a mountainous topology.

Since the sites at a surface exhibit different strengths of interaction with adsorbates and since these sites are present in ordered arrays, we expect adsorbates to bind in well-defined sites. Interactions between adsorbates can enhance the order of the overlayer, indeed, these interactions can also lead to a range of phase transitions in the overlayer.[36] We will discuss the bonding of adsorbates extensively in Chapter 3 and adsorbate–adsorbate interactions in Chapter 4. The symmetry of overlayers of adsorbates may sometimes be related to the symmetry of the underlying surface. We distinguish three regimes: *random adsorption*, *commensurate structures* and *incommensurate structures*. Random adsorption corresponds to the lack of two-dimensional order in the overlayer, even though the adsorbates may occupy (one or more) well-defined adsorption sites. Commensurate structures are formed when the overlayer structure corresponds to the structure of the substrate in some rational fashion. Incommensurate structures are formed when the overlayer exhibits two-dimensional order; however, the periodicity of the overlayer is not related in a simple fashion to the periodicity of the substrate. A more precise and quantitative discussion of the relationship of overlayer to substrate structure is discussed in Section 2.5, which deals with low energy electron diffraction (LEED).

1.2.2 Clean Surface Reconstructions

In most instances, the low index planes of metals are stabilized by simple relaxations. Sometimes relaxation of the selvage is not sufficient to stabilize the surface, as is the case

for Au(111) and Pt(100). To minimize the surface energy, the surface atoms reorganize the bonding among themselves. This leads to surfaces with periodicities that differ from the structure of the bulk terminated surface called *reconstructions*. For semiconductors and polar surfaces it is the rule rather than the exception that the surfaces reconstruct. This can be traced back to the presence of dangling bonds on covalent surfaces whereas metal electrons tend to occupy delocalized states. Delocalized electrons adjust more easily to relaxations and conform readily to the geometric structure of low index planes. Dangling bonds are high-energy entities and solids react in extreme ways to minimize the number of dangling bonds. The step atoms on vicinal surfaces are also associated with localized electronic states, even on metals. In many cases vicinal surfaces are not sufficiently stabilized by simple relaxations and they, therefore, undergo faceting as mentioned above.

One of the most important and interesting reconstructions is that of the Si(100) surface, shown in Figure 1.9, which is the plane most commonly used in integrated circuits. The Si(100)–(2×1) reconstruction completely eliminates all dangling bonds from the original Si(100)–(1×1) surface. The complex Si(111)–(7×7) reconstruction reduces the number of dangling bonds from 49 to just 19. The Wood's notation used to describe reconstructions is explained in Section 2.5.

1.2.3 Adsorbate Induced Reconstructions

An essential tenant of thermodynamics is that at equilibrium a system will possess the lowest possible chemical potential and that all phases present in the system have the same chemical potential. This is true in the real world in the absence of kinetic or dynamic constraints or, equivalently, in the limit of sufficiently high temperature and sufficiently long time so that any and all activation barriers can be overcome. This tenet must also hold for the gas phase/adsorbed phase/substrate system and has several interesting consequences. We have already mentioned that adsorbates can form ordered structures (Figures I. 4, 2.2 and 2.5). This may appear contrary to the wishes of entropy but if an ordered array of sites is to be maximally filled, then the adsorbate must also assume an

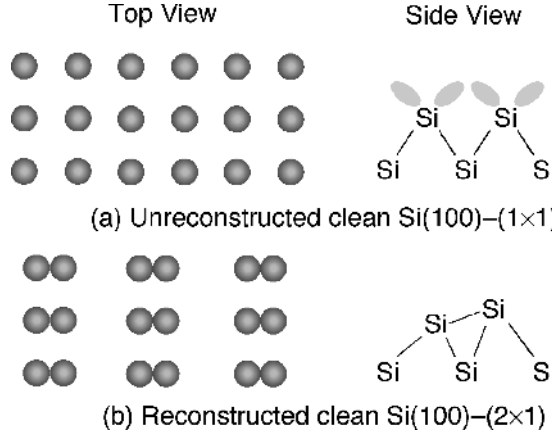

Figure 1.9 *The Si(100)–(2×1) reconstruction: (a) unreconstructed clean Si(100)–(1×1); (b) reconstructed clean Si(100)–(2×1).*

ordered structure. The only constraint on the system is that chemisorption must be sufficiently exothermic to overcome the unfavourable entropy factors.

Adsorbates not only can assume ordered structures, they can also induce reconstruction of the substrate. One way to dispense with dangling bonds is to involve them in bonding. The Si–H bond is strong and nonpolar. H atom adsorption represents a perfect method of capping the dangling bonds of Si surfaces. H atom adsorption is found to *lift the reconstruction* of Si surface, that is, the clean reconstructed surfaces are transformed to a new structure by the adsorption of H atoms. By adsorbing one H atom per surface Si atom, the Si(100)–(2×1) asymmetric dimer structure is changed into a symmetric dimer Si(100)–(2×1):H structure. The Si(111) surface takes on the bulk-terminated (1×1) structure in the presence of chemisorbed hydrogen.

Adsorbate induced reconstructions can have a dramatic effect on the kinetics of reactions on reconstructed surfaces. Of particular importance is the reconstruction of Pt (110). The clean surface is reconstructed into a (1×2) missing row structure, a rather common type of reconstruction. However, CO adsorption leads to a lifting of the reconstruction. Adsorbate induced reconstruction of a metal surface is associated with the formation of strong chemisorption bonds.

The surface does not present a static template of adsorption sites to an adsorbate. Somorjai[37] has collected an extensive list of clean surface and adsorbate induced reconstructions. When an adsorbate binds to a surface, particularly if the chemisorption interaction is strong, we need to consider whether the surface is stable versus reconstruction.[38] For sufficiently strong interactions and high enough adsorbate concentrations we may have to consider whether the surface is stable versus the formation of a new solid chemical compound, such as the formation of an oxide layer, or the formation of a volatile compound, as in the etching of Si by halogen compounds or atomic hydrogen. Here we concentrate on interactions that lead to reconstruction.

The chemical potential of an adsorbate/substrate system is dependent on the temperature T, the chemical identity of the substrate S and adsorbate A, the number density of the adsorbates σ_A and surface atoms σ_S, and the structures assumed by the adsorbate and surface. The gas phase is coupled, in turn, to σ_A through the pressure. Thus, we can write the chemical potential as

$$\mu(T, \sigma_S, \sigma_A) = \sum_i \sigma_{S,i}\mu_i(T) + \sum_j \sigma_{A,j}\mu_j(T). \tag{1.2.1}$$

In Equation (1.2.1) the summations are over the i and j possible structures that the surface and adsorbates, respectively, can assume. The adsorption energy can depend on the surface structure. If the difference in adsorption energy between two surface structures is sufficiently large so as to overcome the energy required to reconstruct the substrate, the surface structure can switch from one structure to the next when a critical adsorbate coverage is exceeded. Note also that Equation (1.2.1) is written in terms of areal densities (the number of surface atoms per unit area) to emphasize that variations in adsorbate concentration can lead to variations in surface structure across the surface. In other words, inhomogeneity in adsorbate coverage may lead to inhomogeneity in the surface structure. An example is the chemisorption of H on Ni(110).[39] Up to a coverage of 1 H atom per surface Ni atom (≡ 1 monolayer or 1 ML), a variety of ordered overlayer structures are formed on the unreconstructed surface. As the coverage increases further,

the surface reconstructs locally into islands that contain 1.5 ML of H atoms. In these islands the rows of Ni atoms pair up to form a (1×2) structure.

Equation (1.2.1) indicates that the equilibrium surface structure depends both on the density (alternatively called coverage) of adsorbates and the temperature. The surface temperature is important in two ways. The chemical potential of each surface structure will depend on temperature. Therefore, the most stable surface structure can change as a function of temperature. Second, the equilibrium adsorbate coverage is a function of the pressure and temperature. Because of this coupling of adsorbate coverage to temperature and pressure, we expect that the equilibrium surface structure can change as a function of these two variables as well as the identity of the adsorbate.[38] This can have important consequences for working catalysts because surface reactivity can change with surface structure.

An example of the restructuring of a surface and the dependence on adsorbate coverage and temperature is the H/Si(100) system (Figure 1.10).[40–43] The clean Si(100) surface reconstructs into a (2×1) structure accompanied by the formation of Si dimers on the surface. The dimers are buckled at low temperature but the rocking motion of the dimer is a low frequency vibration, which means that at room temperature the average position of the dimers appears symmetric. When H adsorbs on the dimer in the monohydride structure (1 H atom per surface Si atom), the dimer becomes symmetric, the dimer bond expands and much of the strain in the subsurface layers is relaxed. Further increasing the H coverage by exposure of the surface to atomic H leads to the formation of dihydride units (SiH_2). These only form in appreciable numbers if the temperature during adsorption is below ~400 K. If the surface is exposed to H at room temperature, trihydride units (SiH_3) can also form. These are a precursor to etching by the formation of SiH_4, which desorbs from the surface. Northrup[44] has shown how these changes are related to the chemical potential and lateral interactions. Neighbouring dihydride units experience repulsive interactions and are unable to assume their ideal positions. This lowers the stability of the fully covered dihydride surface such that some spontaneous formation and desorption of SiH_4 is to be expected.

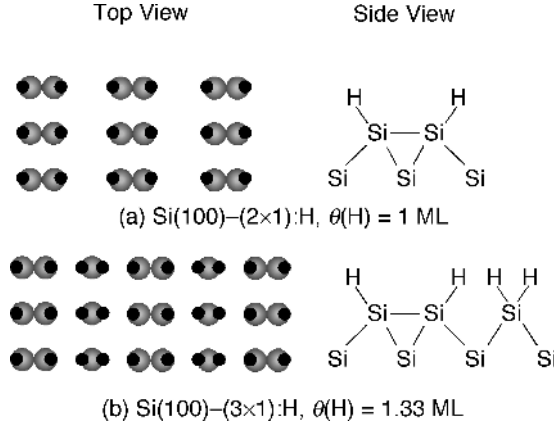

Figure 1.10 *The adsorption of H onto Si(100): (a) Si(100)–(2×1):H, θ(H) = 1 ML; (b) Si (100)–(3×1):H, θ(H) = 1.33 ML. Note: the structures obtained from the adsorption of hydrogen atoms on to Si(100) are a function of the hydrogen coverage, θ(H).1 ML = 1 monolayer as defined by 1 hydrogen atom per surface silicon atom.*

The LEED pattern of a Si(100) surface exposed to large doses of H at room temperature or below has a (1×1) symmetry but it should always be kept in mind that diffraction techniques are very sensitive to order and insensitive to disorder. The (1×1) diffraction pattern has been incorrectly interpreted as a complete coverage of the surface with dihydrides with the Si atoms assuming the ideal bulk termination. Instead, the surface is rough, disordered and composed of a mixture of SiH, SiH_2 and SiH_3 units. The (1×1) pattern arises from the ordered subsurface layers, which are also probed by LEED. If the surface is exposed to H atoms at ~380 K, a (3×1) LEED pattern is observed. This surface is composed of an ordered structure comprised of alternating SiH and SiH_2 units. Thus, there are 3 H atoms for every 2 Si atoms. Heating the (3×1) surface above ~600 K leads to rapid decomposition of the SiH_2 units. The hydrogen desorbs from the surface as H_2 and the surface reverts to the monohydride (2×1) structure.

The reconstructed and nonreconstructed Pt surfaces are shown in Figure 1.11. Of the clean low index planes, only the Pt(111) surface is stable versus reconstruction. The Pt

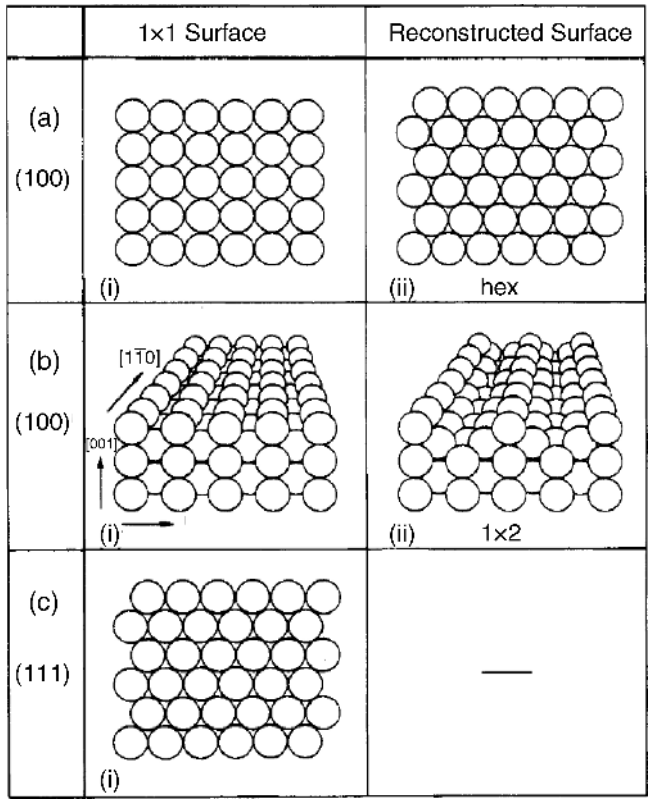

Figure 1.11 *Reconstructed and nonreconstructed surfaces for the three low index planes of Pt: (a) (100) plane, (i) (1 × 1) unreconstructed surface, (ii) quasi-hexagonal (hex) reconstructed surface; (b) (110) plane, (i) (1×1) unreconstructed surface, (ii) missing row (1×2) reconstructed surface; (c) (111) plane, (i) (1×1) unreconstructed surface (Pt(111) is stable against reconstruction). Reproduced from R. Imbihl, G. Ertl, Chem. Rev.* **95**, *697. Copyright (1995), with permission from the American Chemical Society.*

(100) surface reconstructs into a quasi-hexagonal (hex) phase, which is $\sim$40 kJ mol^{-1} more stable than the (1×1) surface. The Pt(110) reconstructs into a (1×2) missing row structure. These reconstructions lead to dramatic changes in the chemical reactivity, which can lead to spatiotemporal pattern formation during CO oxidation (see Chapter 6).[45] The clean surface reconstructions can be reversibly lifted by the presence of certain adsorbates including CO and NO. This is driven by the large difference in adsorption energy between the two reconstructions. For CO the values are 155 and 113 kJ mol^{-1} on the (1×1) and hex phases, respectively, just large enough to overcome the energetic cost of reconstruction.

The surface structure not only affects the heat of adsorption, but it can also dramatically change the probability of dissociative chemisorption. O_2 dissociates with a probability of 0.3 on the Pt(100)–(1×1) surface. On the Pt(100) hex phase, the dissociation probability drops to $\sim 10^{-4}$–10^{-3}. We will investigate the implications of these changes further in Chapter 6. In Chapter 3 we discuss the dynamical factors that affect the dissociation probability.

1.2.4 Islands

A flux of gas molecules strikes a surface at random positions. If no attractive or repulsive interactions exist between the adsorbed molecules (*lateral interactions*), the distribution of adsorbates on the surface would also be random. However, if the surface temperature is high enough to allow for diffusion (Section 3.2), then the presence of lateral interactions can lead to nonrandom distributions of the adsorbates. In particular, the adsorbates can coalesce into regions of locally high concentration separated by low concentration or even bare regions. The regions of high coverage are known as *islands*. Since the coverage in islands is higher than in the surrounding regions, then, according to Equation (1.2.1), the substrate beneath the island might reconstruct whereas regions outside of the islands might not. In some cases, such as H/Ni(110), it is the capacity of a reconstructed region to accommodate a higher coverage than an unreconstructed region that drives the formation of islands. In subsequent chapters, we shall see that islands can have important implications for surface kinetics (Chapter 4), in particular for spatiotemporal pattern formation (Section 6.8) as well as the growth of self-assembled monolayers (Chapter 5) and thin films (Chapter 7).

1.2.5 Chiral Surfaces

One of the great challenges in heterogeneous catalysis is to develop catalysts for *asymmetric synthesis*, that is, catalysts that accelerate the rate of reaction for only one of a pair of enantiomers. Chiral chromatography essentially works because enantiomers (molecules with the same chemical formula but with mirror image structures) have ever so slightly different rates of adsorption and desorption onto and off the surfaces present in the chromatographic column. There are several different ways in which chiral recognition and chemical interaction dependent on chirality can be engineered into surfaces. One is to form a porous solid, the pores or porewalls of which are chiral. Little success in this regard has been achieved with zeolites but recent progress has been made in this area with metal-organic frameworks.[46] Porous solids such as por-Si can be used to immobilize enzymes or chiral molecules.[47] The interactions of these adsorbed species can then be

used for chiral surface processing. Indeed, chiral columns work by means of chiral selectors adsorbed on otherwise achiral surfaces.

Purely two-dimensional structures can also exhibit chiral interactions. The kink sites on vicinal metal surfaces can possess a chiral structure as was first recognized by Gellman and coworkers,[48] who proposed a system for naming left-handed and high-handed kinks $(hkl)^S$ and $(hkl)^R$, respectively. Attard *et al.*[49] were the first to observe that naturally chiral metal surfaces can exhibit entantiospecific chemical reactivity, namely, in the electro-oxidation of glucose on Pt(643)^S. More recently, Greber *et al.*[50] have shown that *D*-cysteine binds 140 meV stronger than *L*-cysteine to the Au(17 11 9)^S kinks on a vicinal Au(111) surface.

Following King and co-workers,[51] we use the *low index* or *singular planes* that contain the highest symmetry elements of each crystal class as the starting point for a description of chiral surfaces. For fcc and bcc crystals these are the {100}, {110} and {111} planes, which contain four-fold, two-fold and three-fold rotational axes, respectively. In an hcp system, the {0001} contains a three-fold rotational axis, while the $\{10\bar{1}0\}$ and $\{11\bar{2}0\}$ planes present two symmetrically distinct two-fold axes. These planes also contain mirror planes. Any plane that contains a mirror plane as a symmetry element is achiral. Any chiral surface will be described by three inequivalent, nonzero Miller indices, such as the (643) and (17 11 9) examples given above.

The (*R*,*S*) naming convention depends on decomposing the kink into the three singular microfacets and assigning an absolute chirality (*R* or *S*) based on the density of atoms in the singular surfaces. King and co-workers[51] have developed a more general (*D*, *L*) naming convention that does not depend on the presence of kinks. Instead, they consider a stereographic projection of the crystal symmetry. They define the surface chirality within a single stereographic triangle (Figure 1.12), by the sense in which one visits the high-symmetry poles at its vertices: proceeding in order of increasing symmetry – {110}, {111}, {100} – a clockwise sequence will imply *D* and an anticlockwise route *L*. For fcc surfaces, the 'D' label is matched with 'R' and the 'L' label is matched with 'S'. This system has the advantage that a general (*hkl*) surface of a primitive cubic crystal will have the same chirality label, regardless of whether the lattice is simple cubic, fcc or bcc.

King *et al.*[51] note that the one-dimensional close-packed chain of atoms is the only extended structural feature shared by all three common metallic crystal forms. They use this construct to define a surface containing two or more such chain directions as 'flat', a surface containing precisely one such direction as 'stepped', and a surface containing no such directions as 'kinked'. Their analysis allows them to draw the following conclusions regarding the symmetry and structure of fcc surfaces: (1) that all chiral surfaces are kinked; (2) that kinked surfaces with one zero index are achiral; (3) that surfaces having two equivalent and nonzero Miller indices are stepped; (4) that the {110} surface is neither more nor less than the most symmetric stepped surface and (5) that only the {111} and {001} surfaces are truly flat. Therefore on fcc crystals, all chiral surfaces are kinked but not all kinked surfaces are chiral.

Similarly for bcc surfaces: (1) all chiral surfaces are kinked, with the exception of those that are merely stepped; (2) stepped surfaces are those with three nonzero indices satisfying $|h| - |k| - |l| = 0$, or an equivalent permutation; (3) all stepped surfaces with three inequivalent indices are chiral and devoid of kinks; (4) kinked surfaces with one or more zero indices or at least two equivalent indices are achiral; (5) the {111} and {001}

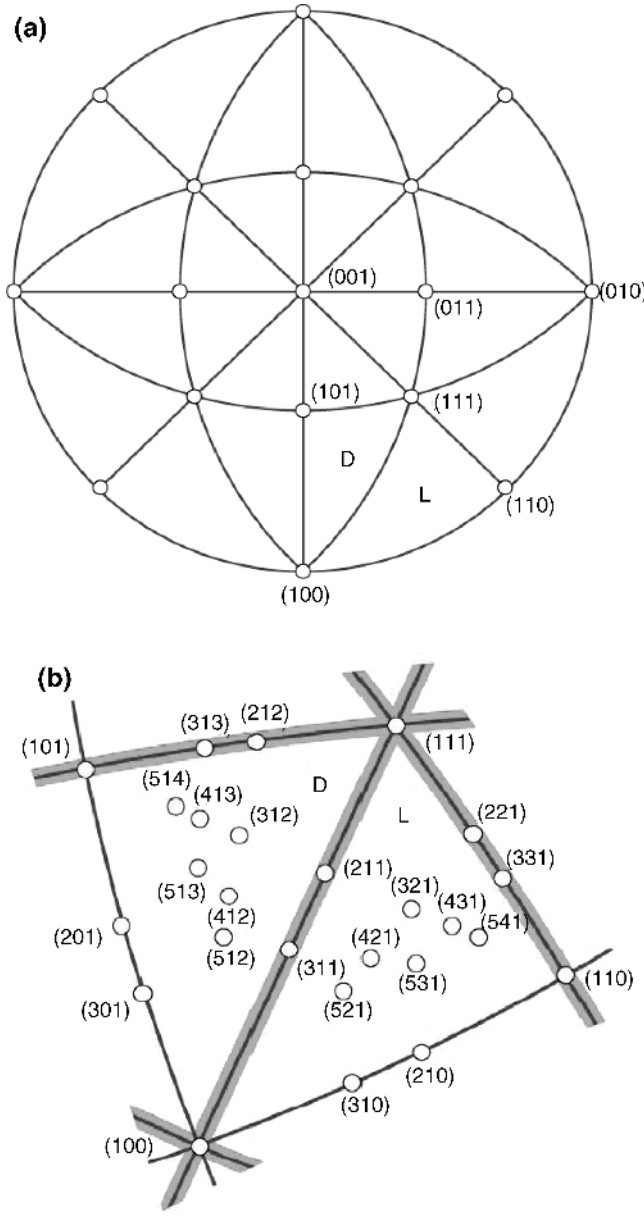

Figure 1.12 *Stereogram projected on (001) showing the mirror zones relevant to primitive fcc, bcc and simple cubic crystal surfaces. Note that right-handed axes are used. The chiralities of two triangles are labelled D and L according to the symmetry-based convention of Pratt et al.*[51] *Reproduced from S.J. Pratt et al., Surf. Sci.,* **585**, *L159. Copyright (2005), with permission from Elsevier.*

surfaces are, in fact, symmetric kinked surfaces; (6) the {211} surface is a symmetric stepped surface analogous to fcc{110} and (7) only the {110} surface is truly flat. On bcc crystal, there are kinked chiral surfaces; however, there are also stepped chiral surfaces that do not have kinks. This is a new class of chiral surfaces that may potentially be more stable than kinked surfaces.

1.3 Band Structure of Solids

1.3.1 Bulk Electronic States

A bulk solid contains numerous electrons. The electrons are classified as being either valence or core electrons. Valence electrons are the least strongly bound electrons and have the highest values of the principal quantum number. Valence electrons form delocalized electronic states that are characterized by three-dimensional wavefunctions known as *Bloch waves*. The energy of Bloch waves depends on the wavevector, k, of the electronic state. The wavevector describes the momentum of the electron in a particular state. Since momentum is a vector, it is characterized by both its magnitude and direction. In other words, the energy of an electron depends not only on the magnitude of its momentum but also, on the direction in which the electron moves. The realm of all possible values of k is known as *k-space*. *k*-space is the world of the solid described in momentum space as opposed to the more familiar world of *xyz* coordinates, known as *real space*.

Because of the great number of electrons in a solid, there are a large number of electronic states. These states overlap to form continuous bands of electronic states and the dependence of the energy on the momentum is known as the *electronic band structure* of the solid. Two bands are always formed: the *valence band* and the *conduction band*. The energetic positions of these two bands and their occupation determine the electrical and optical properties of the solid.

The core electrons are the electrons with the lowest values of the principal quantum number and the highest binding energy. These electrons are strongly localized near the nuclei and they do not form bands. Core electrons are not easily moved from their positions near the nuclei and, therefore, they do not directly participate either in electrical conduction or chemical bonding.

1.3.2 Metals, semiconductors and insulators

The simplest definition of metals, semiconductors and insulators is found in Figure 1.13. In a metal the valence band and the conduction band overlap. There is no energy gap between these bands and the conduction band is not fully occupied. The energy of the highest occupied electronic state (at 0 K) is known as the *Fermi energy*, E_F. At 0 K, all states below the Fermi level (a hypothetical energy level at energy = E_F) are occupied and all states above it are empty. Because the conduction band is not fully occupied, electrons are readily excited from occupied to unoccupied states and the electrons in the conduction band are, therefore, quite mobile. Excitation of an electron from an occupied state to an unoccupied state leads to an excited electronic configuration in which an electron occupies an excited state and an absent electron 'occupies' the original electronic state. This absent electron is known as a *hole*. The hole is a pseudo-particle

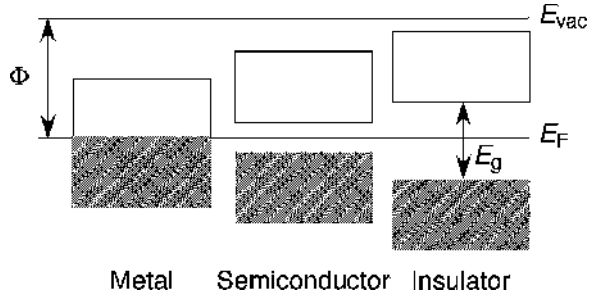

Figure 1.13 *Fermi energies, vacuum energies and work functions in a metal, a semiconductor and an insulator. The presence and size of a gap between electronic states at the Fermi energy, E_F, determines whether a material is a metal, semiconductor or insulator. E_g, bandgap; Φ work function equal to the difference between E_F and the vacuum energy, E_{vac}.*

that acts something like the mirror image of an electron. A hole is effectively a positively charged particle that can be characterized according to its effective mass and its mobility analogous to electrons. Electron excitation always creates a hole. Therefore, we often speak of *electron-hole* (e^--h^+) *pair* formation. As these particles possess opposite charges, they can interact with one another. Creation of electron-hole pairs in the conduction band of metals represents an important class of electronic excitation with a continuous energy spectrum that start at zero energy.

Figure 1.13 illustrates another important property of materials. The vacuum energy, E_{vac}, is defined as the energy of a material and an electron at infinite separation. The difference between E_{vac} and E_F is known as the *work function*, Φ,

$$e\Phi = E_{vac} - E_F. \tag{1.3.1}$$

and at 0 K it represents the minimum energy required to remove one electron from the material to infinity (e is the elementary charge). For ideal semiconductors and insulators, the actual minimum ionization energy is greater than Φ because there are no states at E_F. Instead, the highest energy electrons reside at the top of the valence band. Not apparent in Figure 1.13 is that the work function is sensitively dependent on the crystallographic orientation of the surface, the presence of surface defects in particular steps[5, 52] and, of course, the presence of chemical impurities on the surface.

The reason for the dependence of the work function on surface properties can be traced back to the electron distribution at the surface (Figure 1.14). The electron density does not end abruptly at the surface. Instead, the electron density oscillates near the surface before decaying slowly into the vacuum (*Friedel oscillations*). This distribution of electrons creates an electrostatic dipole layer at the surface. The *surface dipole* contribution D is equal to the difference between the electrostatic potential energy far into the vacuum and the mean potential deep in the bulk,

$$D = V(\infty) - V(-\infty). \tag{1.3.2}$$

If we reference the electrostatic potential with respect to the mean potential in the bulk, i.e. $V(-\infty) = 0$, then the work function can be written

$$e\Phi = D - E_F. \tag{1.3.3}$$

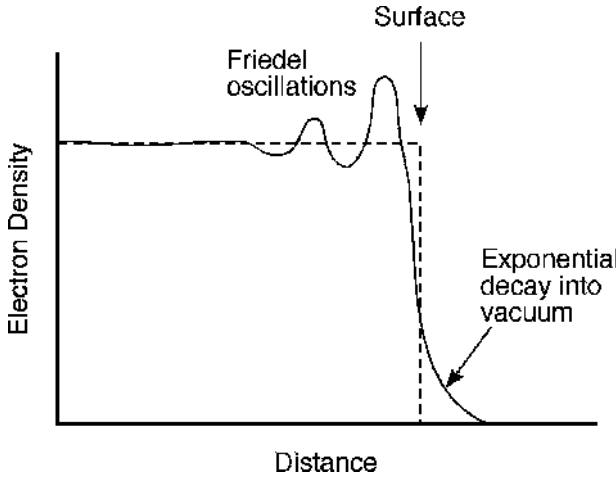

Figure 1.14 *Friedel oscillations: the electron density near the surface oscillates before decaying exponentially into the vacuum.*

Therefore, Φ is determined both by a surface term D and a bulk term E_F. With this definition of the work function, changes in D due to surface structure and adsorbates are responsible for changes in Φ because surface properties cannot affect E_F. More commonly, the work function is given in units of eV and Equation (1.3.3) is written as

$$\Phi = -e\chi - \frac{E_F}{e} \tag{1.3.4}$$

where χ is the *surface potential* in volts (the electrostatic potential step resulting from the inhomogeneous charge distribution at the surface) and E_F is in joules. On metal surfaces χ is negative.

The occupation of electronic states is governed by Fermi-Dirac statistics. All particles with noninteger spin such as electrons, which have a spin of $1/2$, obey the *Pauli exclusion principle*. This means that no more than two electrons can occupy any given electronic state. The energy of electrons in a solid depends on the availability of electronic states and the temperature. Metals sometimes exhibit regions of k-space in which no electronic states are allowed. These forbidden regions of k-space are known as *partial bandgaps*. At finite temperature, electrons are not confined only to states at or below the Fermi level. At equilibrium they form a reservoir with an energy equal to the chemical potential, μ. The probability of occupying allowed energy states depends on the energy of the state, E, and the temperature according to the *Fermi-Dirac distribution*

$$f(E) = \frac{1}{\exp[(E-\mu)/k_B T] + 1}. \tag{1.3.5}$$

The Fermi-Dirac distribution for several temperatures is drawn in Figure 1.15. At $T = 0\,\mathrm{K}$, the Fermi-Dirac function is a step function, that is $f(E) = 1$ for $E < \mu$ and $f(E) = 0$ for $E > 0$. At this temperature the Fermi energy is identical to the *chemical potential*

$$\mu(T = 0\mathrm{K}) \equiv E_F. \tag{1.3.6}$$

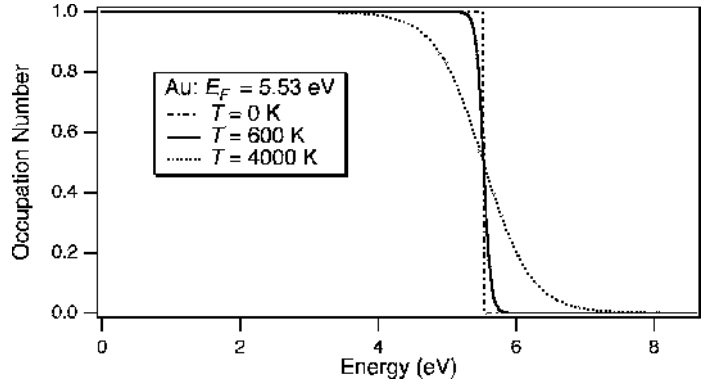

Figure 1.15 *Fermi-Dirac distribution for gold at three different temperatures, T. E_F, Fermi energy.*

More generally, the chemical potential is defined as the energy at which $f(E) = 0.5$. It can be shown (see for instance Elliot,[53] that

$$\mu(T) \approx E_{\mathrm{F}}\left[1 - \frac{\pi^2}{12}\left(\frac{k_{\mathrm{B}}T}{E_{\mathrm{F}}}\right)^2\right]. \tag{1.3.7}$$

A direct consequence of Fermi-Dirac statistics is that the Fermi energy is not zero at 0 K. In fact, E_{F} is a material dependent property that depends on the electron density, ρ, according to

$$E_{\mathrm{F}} = \frac{h^2}{2m_{\mathrm{e}}}(3\pi^2\rho)^{2/3}. \tag{1.3.8}$$

E_{F} is on the order of several eV and $E_{\mathrm{F}}/k_{\mathrm{B}}$, known as the *Fermi temperature*, T_{F}, is on the order of several thousand Kelvin. Consequently, the chemical potential and E_{F} are virtually identical unless the temperature is extremely high.

Semiconductors exhibit a complete bandgap between the valence and conduction bands. The energy of the *conduction band minimum* is E_{C} and the energy at the *valence band maximum* is E_{V}. The magnitude of the bandgap is the difference between these two:

$$E_{\mathrm{g}} = E_{\mathrm{C}} - E_{\mathrm{V}}. \tag{1.3.9}$$

The Fermi level of a pure semiconductor, known as an *intrinsic semiconductor*, lies in the bandgap. The exact position depends on the temperature according to

$$E_{\mathrm{F}} = E_{\mathrm{i}} = \frac{E_{\mathrm{C}} + E_{\mathrm{V}}}{2} + \frac{k_{\mathrm{B}}T}{2}\ln\left(\frac{N_{\mathrm{V}}}{N_{\mathrm{C}}}\right), \tag{1.3.10}$$

where N_{V} and N_{C} are the effective densities of states of the valence and conduction bands, respectively. The densities of states can be calculated from material specific constants and the temperature as shown, for instance, by Sze.[54] Equation (1.3.10) shows that the Fermi energy of an intrinsic semiconductor lies near the middle of the gap. As we shall see below, this is not true for the more common case of a doped (extrinsic) semiconductor.

In the bulk of a perfect semiconductor there are no electrons at the Fermi level, even though it is energetically allowed, because there are no allowed electronic states at this energy. An equivalent statement is that in the bulk of an ideal semiconductor, the *density of states* is zero at E_F. In any real semiconductor, *defects* (structural irregularities or impurities) introduce a non-zero density of states into the bandgap. These states are known as *gap states*. At absolute zero the valence band is completely filled and the conduction band is completely empty. At any finite temperature, some number of electrons is thermally excited into the conduction band. This number is known as the *intrinsic carrier density* and is given by

$$n_i = \sqrt{N_C N_V}\exp(-E_g/2k_BT) \tag{1.3.11}$$

The presence of a bandgap in a semiconductor means that the electrical conductivity of a semiconductor is low. The bandgap also increases the minimum energy of electron-hole pair formation from zero to $\geq E_g$. What distinguishes a semiconductor from an insulator is that E_g in a semiconductor is sufficiently small that either thermal excitations or the presence of impurities can promote electrons into the conduction band or holes into the valence band. Electrically active impurities are known as *dopants*. There are two classes of dopants. If a valence III atom, such as B, is substituted for a Si atom in an otherwise perfect Si crystal, the B atom accepts an electron from the Si lattice. This effectively donates a hole into the valence band. The hole is mobile and leads to increased conductivity. B in Si is a *p-type dopant* because it introduces a *positive* charge carrier into the Si band structure. B introduces acceptor states into the Si and the concentration of acceptor atoms is denoted N_A. On the other hand if a valence V atom, such as P, is doped into Si, the P atom effectively donates an electron into the conduction band. Because the resulting charge carrier is *negative*, P in Si is known as an *n-type dopant*. Analogously, the concentration of donors is N_D.

The position of the Fermi energy in a doped semiconductor depends on the concentration and type of dopants. E_F is pushed upward by *n*-type dopants according to

$$E_F = E_i + k_BT\ln\left(\frac{N_D}{n_i}\right). \tag{1.3.12}$$

In a *p*-type material, E_F is pulled toward the valence band

$$E_F = E_i - k_BT\ln\left(\frac{N_A}{n_i}\right). \tag{1.3.13}$$

Equations (1.3.12) and (1.3.13) hold as long as the dopant density is large compared with the n_i and density of electrically active dopants of the opposite type.

An insulator has a large bandgap. The division between a semiconductor and an insulator is somewhat arbitrary. Traditionally, a material with a bandgap larger than $\sim$3 eV has been considered to be an insulator. The push of high technology and the desire to fabricate semiconductor devices that operate at high temperatures has expanded this rule of thumb. Hence diamond with a bandgap of $\sim$5.5 eV now represents the upper limit of wide bandgap semiconductors.

Graphite represents one other important class of material. It does have electronic states up to the Fermi energy. However, the conduction and valence band edges, which correlate with π^* antibonding and π bonding bands formed from p_z-like orbitals, only overlap in a

small region of k space. Therefore, the density of states at E_F is minimal and graphite is considered a semi-metal.

1.3.3 Energy Levels at Metal Interfaces

An interface is generally distinguished from a surface as it is thought of as the boundary between two materials (or phase) in intimate contact. At equilibrium, the chemical potential must be uniform throughout a sample. This means that the Fermi levels of two materials, which are both at equilibrium and in electrical contact, must be the same.

Figure 1.16 demonstrates what occurs when two bulk metals are brought together to form an interface. In Figure 1.16(a) we see that two isolated metals share a common vacuum level but have different Fermi levels, E_F^L and E_F^R, as determined by their work functions, Φ_L and Φ_R. L and R refer to the left-hand and right-hand metals, respectively. When the two metals are connected electrically electrons flow from the low work function metal to the high work function metal, L $\rightarrow$ R, until the Fermi levels become equal. Consequently, metal L is slightly depleted of electrons and metal R has an excess. In other words, a dipole develops between the two metals and with this is associated a small potential drop, the *contact potential*

$$\Delta\varphi = \Phi_R - \Phi_L, \tag{1.3.14}$$

and an electrical field. The presence of the electric field is evident in Figure 1.16(b) by the sloping vacuum level. Figure 1.16 demonstrates that the bulk work functions of the two metals remain constant. Since the Fermi energies must be equal at equilibrium, the vacuum level shifts in response.

In metals, *screening* of free charges by valence electrons is efficient. Screening is the process by which the electrons surrounding a charge (or charge distribution such as a dipole) are polarized (redistributed) to lower the energy of the system. Screening is not very effective in insulators because the electrons are not as free to move. Therefore, when

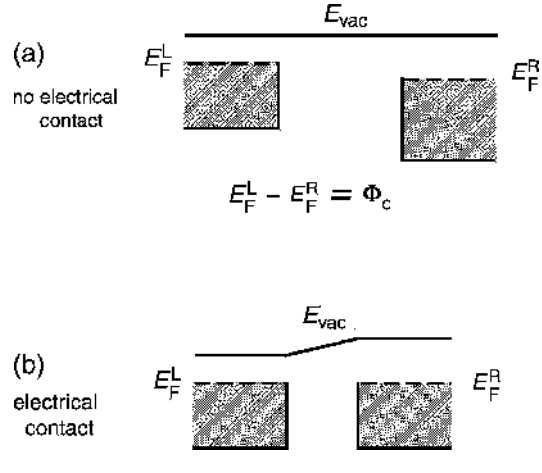

Figure 1.16 *Electronic bands of metals (a) before and (b) after electrical contact. The Fermi energies of the two metals align at equilibrium when electrical contact is made. E_{vac}, vacuum energy; E_F, Fermi energy; subscripts L and R refer to left-hand and right-hand metal, respectively.*

the two metals are actually brought into contact, the width of this dipole layer is only a few angstroms. The energetic separation between E_F and E_{vac} is constant after the first two or three atomic layers. At the surface, however, this separation is not constant. For the interface of two metals this means that the position of E_{vac} does not change abruptly but continuously.

The presence of a dipole layer at the surface has other implications for clean and adsorbate covered surfaces. The difference between E_F and E_{vac} in the bulk is a material specific property. In order to remove an electron from a metal, the electron must pass through the surface and into the vacuum. Therefore if two samples of the same metal have different dipole layers at the surface, they exhibit different work functions. In Fig. 1.5 we have seen that Smoluchowski smoothing at steps introduces dipoles into the surface. A linear relationship between *step* density and work function decrease has been Observed.[52] Similarly, the geometric structure of the surface determines the details of the electronic structure at the surface. Thus, the work function is found to depend both on the crystallographic orientation of the surface as well as the presence of surface reconstructions.

The presence of adsorbates on the surface of a solid can introduce two distinct dipolar contributions to the work function. The first occurs if there is charge transfer between the adsorbate and the surface. When an electropositive adsorbate such as an alkali metal forms a chemical bond with a transition metal surface, the alkali metal tends to donate charge density into the metal and decreases the work function. An electronegative adsorbate, such as O, S or halogens, withdraws charge and increases the work function. The second contribution arises when a molecular adsorbate has an intrinsic dipole. Whether this contribution increases or decreases the work function depends on the relative orientation of the molecular dipole with respect to the surface.

1.3.4 Energy Levels at Metal–Semiconductor Interfaces

The metal–semiconductor interface is of great technological importance not only because of the role it plays in electronic devices.[54] Many of the concepts developed here are also directly applicable to charge transfer at the electrolyte–semiconductor interface.[55,56] It is somewhat more complicated than the metal–metal interface but our understanding of it can be built up from the principles that we have learned above. The situation is illustrated in Figure 1.17. Again the Fermi levels of the metal and the semiconductor must be aligned at equilibrium. Equalization of E_F is accomplished by charge transfer. The direction of charge transfer depends on the relative work functions of the metal (M) and the semiconductor (S). The case of $\Phi_S > \Phi_M$ for an *n*-type semiconductor is depicted in Figure 1.17(a), whereas $\Phi_S < \Phi_M$ is depicted in Figure 1.17(b). Screening in a semiconductor is much less effective, which results in a near-surface region of charge density different from that of the bulk with a width of several hundred angstroms. This is called a *space-charge region*. In Figure 1.17(a) the metal has donated charge to the semiconductor space-charge region. The enhanced charge density in the space-charge region corresponds to an *accumulation layer*. In Figure 1.17(b) charge transfer has occurred in the opposite direction. Because the electron density in this region is lower than in the bulk, this type of space-charge region is know as a *depletion layer*. The shape of the space-charge region has a strong influence on carrier transport in

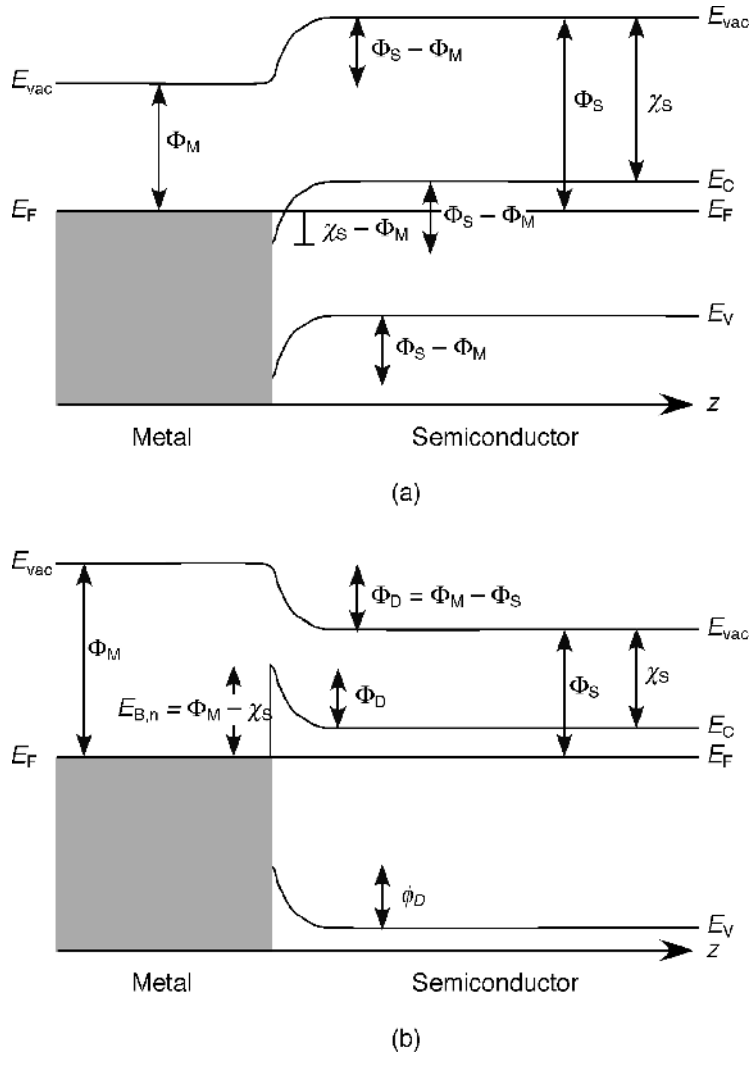

Figure 1.17 *Band bending in an n-type semiconductor at a heterojunction with a metal. (a) Ohmic contact ($\Phi_S > \Phi_M$). (b) Blocking contact (Schottky barrier, $\Phi_S < \Phi_M$). The energy of the bands is plotted as a function of distance z in a direction normal to the surface. Φ_S, Φ_M work function of the semiconductor and of the metal, respectively; E_{vac}, vacuum energy; E_C, energy of the conduction band minimum; E_F, Fermi energy; E_V energy of the valence band maximum. Redrawn from S. Elliott, The Physics and Chemistry of Solids. (1998) Copyright, with permission from John Wiley & Sons, Ltd.*

semiconductors and the electrical properties of the interface. Figure 1.17(a) corresponds to an *ohmic contact* whereas Figure 1.17(b) demonstrates the formation of a *Schottky barrier*.

In the construction of Figure 1.17 we have introduced the *electron affinity* of the semiconductor, χ_S. This quantity as well as the *bandgap* remain constant throughout the

semiconductor. Importantly, the positions of the band edges at the surface remain constant. Thus we see that the differences E_{vac}–E_V and E_{vac}–E_C are constant whereas the positions relative to E_F vary continuously throughout the space-charge region. The continuous change in E_V and E_C is called *band bending*.

E_{vac}, E_C and E_V all shift downward by the same amount in Figure 1.17(a). In Figure 1.17(b) the shifts are all upward but again E_{vac}, E_C and E_V all shift by the same amount. The potential at the surface is the magnitude of the band bending and is given by

$$eU_{surf} = E_{vac}^{surf} - E_{vac}^{bulk}. \tag{1.3.15}$$

In Equation (1.3.15) E_{vac} was chosen but the shifts in E_{vac}, E_C and E_V are all the same, hence any one of these three could be used in Equation (1.3.15). The doping density determines the magnitude of the band bending and the *depletion layer width*, d. For an n-type semiconductor, the value is

$$U_{surf} = -\frac{eN_D d^2}{2\varepsilon\varepsilon_0}, \tag{1.3.16}$$

where ε and ε_0 are the permittivities of the semiconductor and free space. In a p-type semiconductor, the sign is reversed and N_A is substituted for N_D. From Figure 1.17 it is further apparent that

$$U_{surf} = \Phi_S - \Phi_M \quad \text{(Ohmic as in Figure1.17(a))} \tag{1.3.17}$$

and

$$U_{surf} = \Phi_M - \chi_S \quad \text{(Schottky as in Figure1.17(b))} \tag{1.3.18}$$

for n-type Ohmic and Schottky contacts, respectively. U_{surf} in the case of a Schottky contact is also known as the *Schottky barrier* height.

Of great importance for both device applications and for electrochemistry is that the extent of band bending can be changed by the application of an external bias. When a voltage U is applied across a semiconductor junction (either metal–semiconductor or electrolyte–semiconductor) it is not the *chemical potential* that is constant throughout the junction region but the *electrochemical potential*, $\bar{\mu}$

$$\bar{\mu} = \mu - eU, \tag{1.3.19}$$

as shown in Figure 1.18. In *forward bias* electrons flow from the semiconductor to the metal and the barrier is reduced by eU. In *reverse bias*, little current flows from the metal into the semiconductor as the barrier height is increased by eU. The potential at which $\mu - eU = 0$ is known as the *flatband potential* U_{FB}, and therefore

$$U_{FB} = \mu/e, \tag{1.3.20}$$

from which the *Fermi level* of the semiconductor can be determined.

1.3.5 Surface Electronic States

All atoms in the bulk of a pure metal or elemental semiconductor are equivalent. The atoms at the surface are, by definition, different because they do not possess their full complement of bonding partners. Therefore surface atoms can be thought of as a type of impurity. Just as impurities in the bulk can have localized electronic states associated

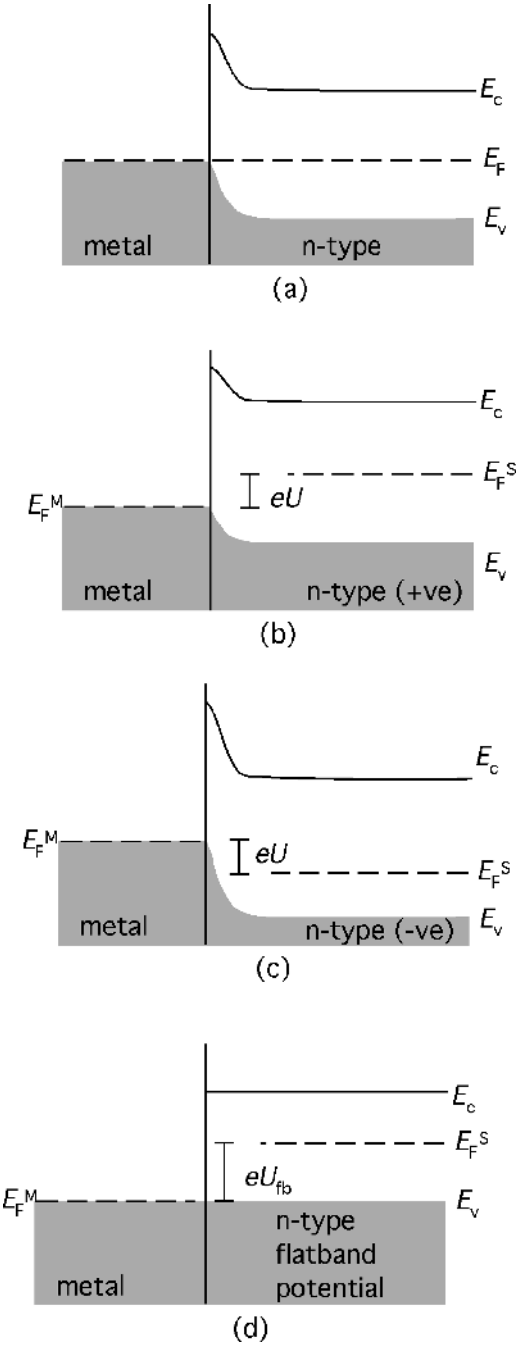

Figure 1.18 *The electrochemical potential and the effects of an applied voltage on a metal–semiconductor interface. (a) No applied bias. (b) Forward bias. (c) Reverse bias. (d) Biased at the flatband potential, U_{fb}. E_C, energy of the conduction band minimum; E_F, Fermi energy; E_V, energy of the valence band maximum; superscripts M and S refer to the metal and the semiconductor, respectively.*

with them, so too can surface atoms. We need to distinguish two types of electronic states associated with surface atoms. An electronic state that is associated with the surface can either overlap in *k*-space with bulk states or it can exist in a bandgap. An overlapping state is known as a *surface resonance*. A surface resonance exists primarily at the surface; nonetheless, it penetrates into the bulk and interacts strongly with the bulk electronic states. A *true surface state* is strongly localized at the surface and because it exists in a bandgap, it does not interact strongly with bulk states. A surface state or resonance can either be associated with surface atoms of the solid (*intrinsic surface state* or resonance) or with adsorbates (*extrinsic surface state* or resonance). Structural defects can also give rise to surface states and resonances. Surface states and surface resonances are illustrated in Figure 1.19.

Surface states play a defining role in determining the surface band structure of semiconductors. In effect, they can take the place of the metal and the reasoning we used in Section 1.3.4 can be used to describe band bending in the presence of surface states. If the electron distribution in a semiconductor were uniform all the way to the surface, the bands would be flat. The presence of surface states means that the surface may possess a greater or lesser electron density relative to the bulk. This nonuniform electron distribution again leads to a space-charge region and band bending. Surface states can either act as donor or acceptor states. Surface states can have a strong influence on the electrical properties of devices, in particular, on the behaviour of Schottky barriers.[53,54,57]

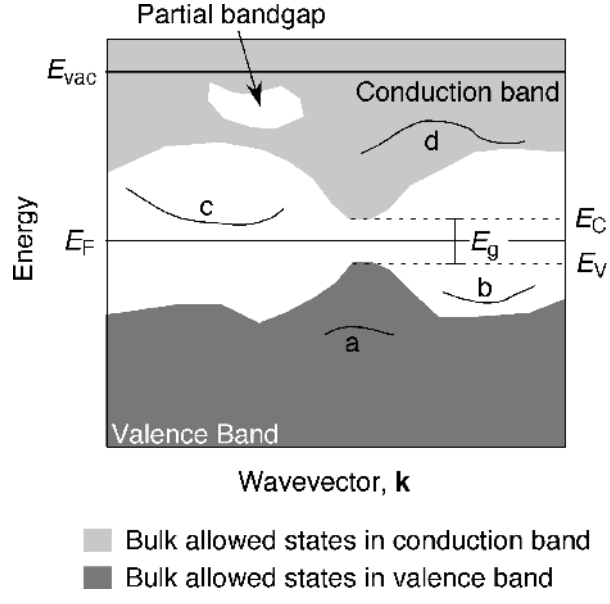

Figure 1.19 *The band structure of a semiconductor, including an occupied surface resonance (a), an occupied surface state (b), a normally unoccupied surface state (c) and a normally unoccupied surface resonance (d). E_{vac}, vacuum energy; E_F, Fermi energy; E_V, energy of the valence band maximum; E_C, the conduction band minimum.*

The distinction between a resonance and a state may seem somewhat arbitrary. The difference is particularly obvious in normally unoccupied or empty states that exist above the Fermi level. *Empty states* can be populated by the absorption of photons with energies less than the work function. The strong interaction between bulk states and a resonance results in a short lifetime for electrons excited into the resonance. A surface state exhibits a much longer lifetime. These lifetimes have been measured directly by two photon photoemission (Section 2.6.3). Lifetimes depend on the specific system. For example, on Si(111)–(2×1) the π^* normally unoccupied surface state has a lifetime of $\sim$200 ps.[58]

If in a metal an energy gap exists somewhere between E_F and E_{vac}, an electron excited into this gap experiences an attractive force associated with its image potential. The result is a series of bound states, *image potential states*,[59,60] that are the surface analogue of Rydberg states in atomic and molecular systems. To a first approximation,[60] the energies of these states form a series whose energy is given by

$$E_n = -\frac{R_\infty}{16n^2} = -\frac{0.85\,\text{eV}}{n^2} \tag{1.3.21}$$

converging on the energy of the vacuum level, E_{vac}. These states are bound in the z direction (normal to the surface) but are free electron like in the plane of the surface. As n increases, the wavefunction of the image states overlaps less and less with the bulk leading to progressively less interaction between the two. The result is that the lifetime of the state increases with n. This has been measured directly by Höfer *et al.*[61] who have found that above Cu(100) the lifetime varies from 40±6 to 300±15 fs as n changes from 1 to 3. Similarly, the lifetime can be increased by the introduction of a spacer layer between the image state and the metal surface. Wolf, Knoesel and Hertel[62] have shown that the presence of a physisorbed Xe layer increases the $n = 1$ lifetime on Cu(111) from 10±3 fs to 50±10 fs.

1.3.6 Size Effects in Nanoscale Systems

Above we have confined our discussion to extended, essentially semi-infinite solids. We have seen that the surface acts differently than the bulk. What happens if we shrink our sample from a semi-infinite solid to a finite cluster of atoms? Table 1.2 lists several characteristics of cluster and classifies them arbitrarily along the lines of small, medium and large clusters. We can see that the relative number of surface atoms N_s, compared with the total number of atoms in the cluster N, changes as a function of cluster size. Therefore, the relative important of the surface for determining the properties of the cluster changes as a function of size. Because surface atoms act differently than bulk atoms, this also means that the properties of the cluster will change as a function of size, that is, as a function of the number of atoms in the cluster. Small clusters are close to molecular in their behaviour with electronic states that are discreet or approaching discreet behaviour. Their properties do not change regularly with decreasing size. Large clusters have smoothly varying properties that are approaching bulk values. Different properties (vapour pressure, ionization potential, polarizability, etc.) may change at different rates, with some having already attained bulk values and other still exhibiting size dependent behaviour. Medium sized clusters have electronic states that are approaching the band like states of large clusters, but which are still distinctly different from the bulk states. The properties of the cluster generally vary in a smooth function as a function of size.

Table 1.2 *Clusters can be roughly categorized on the basis of their size. The properties of clusters depend on size. For clusters of different composition the boundaries might occur as slightly different values. The diameter is calculated on the assumption of a close packed structure with the atoms having the size of a Na atom.*

	Small	**Medium**	**Large**
Atoms (N)	2–20	20–500	500–10^6
Diameter/nm	≤ 1.1	1.1–3.3	3.3–100
Surface/Bulk (N_s/N)	Not separable	0.9–0.5	≤ 0.5 ~ 0.2 for $N = 3000$ $\ll 1$ for $N \geq 10^5$
Electronic states	Approaching discrete	Approaching bands	Moving toward bulk behaviour
Size dependence	No simple, smooth dependence of properties on size and shape	Size dependent properties that vary smoothly	Quantum size effects may still be important but properties approaching bulk values

What separates clusters, also called *nanoparticles*, from bulk materials is that their properties are size dependent. A glass of pure water has a well-defined melting point of 273 K. The amount of energy required to remove a molecule of water from the surface of liquid water (the desorption energy) is also well defined. Half a glass of water also has the same melting point and desorption energy. This is not true of water clusters. The melting point of a water cluster $(H_2O)_N$ with $N = 10$ is not the same as for $N = 100$. Similarly, the amount of energy required to desorb a water molecule from $(H_2O)_{10}$ is not the same as for $(H_2O)_{100}$. This regime of size dependent properties is the hallmark of nanoscience, which challenges our conception of what something is because a very small nanoglass of water does not behave the same as a macroscopic glass of water.

One reason for size dependent properties is the aforementioned change in the number of surface atoms to bulk atoms, or stated more generally when surface contributions begin to dominate bulk contributions to cluster properties. A second reason is *quantum confinement*. Quantum confinement can be defined as the phenomenon of when a particle knows the size of its container. The pertinent size of a particle is given by its *de Broglie wavelength* λ,

$$\lambda = h/p, \tag{1.3.22}$$

where h is the Planck constant and $p = mv$ is the linear momentum. When the container that confines a particle approaches the size of its de Broglie wavelength, the properties of the particle become dependent on the size of the container. For excited electrons in a solid an *exciton* radius can be defined. When the size of the particle approaches the size of the exciton, the electronic structure becomes size dependent. For Si, the onset of size dependent electronic structure is around 5 nm.

Perhaps the easiest example to consider is that of a *particle in a box*. If the box has a length L and the walls are impenetrable (the potential energy goes to infinity at $x = 0$ and $x = L$), the energy levels of the box are given by

$$E_n = \frac{n^2 h^2}{8mL^2}, n = 1, 2, 3, \ldots \tag{1.3.23}$$

The important things to draw from Equation (1.3.23) are that the energy levels are quantized (n is an integer not a continuum variable) and spacing between levels ΔE is inversely proportional to particle mass and the length of the box squared

$$\Delta E \propto \frac{1}{mL^2}. \tag{1.3.24}$$

When thermal excitations are greater than the spacing between levels, that is $k_B T \gg \Delta E$, quantum effects are smeared out and systems behave in the continuum fashion familiar to classical mechanics. Systems for which quantum effects are important are those for which $\Delta E \gtrsim k_B T$. Large values of ΔE are favoured by small m and small L. Quantum confinement is, therefore, most likely to affect light particles confined to small boxes, especially at low temperature. Sufficiently small particles will exhibit quantum effects even at room temperature and above.

1.4 The Vibrations of Solids

1.4.1 Bulk Systems

The vibrations of a solid are much more complex than the vibrations of small molecules. This arises from the many-body nature of the interactions of atoms in a solid. Analogous to electronic states, the vibrations of a solid depend not only on the movements of atoms, but also on the direction in which the atoms vibrate. The multitudinous vibrations of the solid overlap to form a *phonon* band structure, which describes the energy of phonons as a function of a wavevector. Partial bandgaps can be found in the phonon band structure. Within the *Debye model*,[53] there is a maximum frequency for the phonons of a solid, the *Debye frequency*. The Debye frequency is a measure of the rigidity of the lattice. Typical values of the Debye frequency are 14.3 meV (115 cm^{-1}) and 34.5 meV (278 cm^{-1}) for Au and W, respectively and 55.5 meV (448 cm^{-1}) for Si. The most rigid lattice is that of diamond which has a Debye frequency of 192 meV (1550 cm^{-1}). Note that the Debye frequency is the highest frequency obtainable within the model but that real crystals may exhibit slightly higher values. For instance the highest longitudinal optical phonon mode of Si lies at 520 cm^{-1}.

From the familiar *harmonic oscillator* model, the energy of a vibrational normal mode in an isolated molecule is given by

$$E_v = (v + 1/2)\hbar\omega_0 \tag{1.4.1}$$

where v is the vibrational quantum number and w_0 is the fundamental radial frequency of the oscillator.

In a 3D crystal with harmonic vibrations, this relationship needs to be modified in two important ways. First we note that a crystal is composed of N primitive cells containing p atoms. Since each atom has three translational degrees of freedom, a total of $3pN$ vibrational degrees of freedom exist in the solid. The solutions of the wave equations for vibrational motion in a periodic solid can be decomposed in $3p$ *branches*. Three of these modes correspond to *acoustic modes*. The remaining $3(p–1)$ branches correspond to *optical modes*. Optical modes can be excited by the electric field of an electromagnetic wave if the excitation leads to a change in dipole moment. Acoustic and optical modes

are further designated as being either transverse or longitudinal. *Transverse modes* represent vibrations in which the displacement is perpendicular to the direction of propagation. The vibrational displacement of *longitudinal modes* is parallel to the direction of propagation.

The second important modification arises from the 3D structure of the solid. Whereas the vibrations of a molecule in free space do not depend on the direction of vibration, this is not the case for a vibration in an ordered lattice. This is encapsulated in the use of the *wavevector* of the vibration. The wavevector is given by

$$|\boldsymbol{k}| = \frac{2\pi}{\lambda}, \tag{1.4.2}$$

where λ is the wavelength and $\boldsymbol{k}$ is a vector parallel to the direction of propagation. Consistent with this definition, we introduce the radial frequency of the vibration, ω_k,

$$\omega_k = 2\pi\upsilon_k. \tag{1.4.3}$$

We now write the energy of a vibration of wavevector $\boldsymbol{k}$ in the pth branch as

$$E(\boldsymbol{k}, p) = (n(\boldsymbol{k}, p) + 1/2)\hbar\omega_k(p). \tag{1.4.4}$$

The vibrational state of the solid is then represented by specifying the excitation numbers, $n(\boldsymbol{k}, p)$, for each of the $3pN$ normal modes. The total vibrational energy is thus a sum over all of the excited vibrational modes

$$E = \sum_{k,p} E(\boldsymbol{k}, p). \tag{1.4.5}$$

By direct analogy to the quantized electromagnetic field, it is conventional to describe the vibrations of a solid in terms of particle-like entities (*phonons*) that represent quantized elastic waves. Just as for diatomic molecules, Equations (1.4.4) and (1.4.5) show that the vibrational energy of a solid is non-vanishing at 0 K as a result of zero point motion.

The mean vibrational energy (see Exercise 1.5) is given by

$$\langle E \rangle = 1/2\omega_k(p) + \frac{\hbar\omega_k(p)}{\exp(\hbar\omega_k(p)/k_\mathrm{B}T) - 1}. \tag{1.4.6}$$

Thus by comparison to Eq. (1.4.4), it is confirmed that the *mean phonon occupation number* is

$$n(\boldsymbol{k}, p) \equiv \langle n(\omega_k(p), T) \rangle = \frac{1}{\exp(\hbar\omega_k(p)/k_\mathrm{B}T) - 1} \tag{1.4.7}$$

and that it follows the *Planck distribution law*. This is expected for bosons, that is, particles of zero (more generally, integer) spin. Accordingly, the number of phonons in any given state is unlimited and determined solely by the temperature.

Again in analogy to electronic states, there are phonon modes that are characteristic of and confined to the surface. *Surface phonon modes* have energies that are well defined in k-space and sometimes exist in the partial bandgaps of the bulk phonons. Surface phonon modes that exist in bandgaps are true surface phonons, whereas those that overlap with bulk phonon in k-space are surface phonon resonances. Furthermore, since the surface atoms are under-coordinated compared with the bulk, the *surface Debye frequency* is routinely much lower than the bulk Debye frequency. In particular, the vibrational

amplitude perpendicular to the surface is much larger for surface than for bulk atoms. Depending on the specific material, the root mean square vibrational amplitudes at the surface are commonly 1.4–2.6 times larger on surfaces than in the bulk.

1.4.2 Nanoscale Systems

Just as the electronic properties of a system become size dependent in the nanoscale regime, so too do the vibrational properties. This is most conveniently probed through the vibrational Raman spectrum. The peak position as well as the peak shape depend not only on the size of the crystallite probed[63] but also its shape.[64,65] There is still no comprehensive theory of the lattice dynamics of nanostructures. The theoretical approaches can be classified as either continuum models[66] or lattice dynamical models.[65]

The Raman spectrum probes the optical phonons of the sample. For a large sample only the $q = 0$ phonons at the centre of the Brillouin zone are probed in the first order spectrum, where q is the momentum of the phonon in units of $2\pi/a$ and a is the lattice constant. As the sample size is reduced, the $q = 0$ selection rule is relaxed. This will lead to a shift in the peak centre and a broadening of the peak, both of which are dependent on the phonon dispersion, that is, on the function $\omega(q)$ which details how the phonon frequency depends on momentum. For spherical nanocrystals of diameter L, the intensity of first-order Raman spectrum $I(\omega, L)$ is given by

$$I(\omega, L) = \int \frac{\exp(-q^2L^2/2\alpha)}{[\omega(q) - \omega]^2 + (\Gamma_0/2)^2} d^3q. \tag{1.4.8}$$

For a sample of nanoparticles[67] with a size distribution described by the function $\varphi(L)$, the experimentally observed Raman spectrum will be described by a convolution of the intensity function of Equation (1.4.8) with $\varphi(L)$ according to

$$I(\omega) = \int \varphi(L) I'(\omega, L) dL. \tag{1.4.9}$$

1.5 Summary of Important Concepts

- Ideal flat surface are composed of regular arrays of atoms with an areal density on the order of $10^{15}\,\mathrm{cm}^{-2}$ ($10^{19}\,\mathrm{m}^{-2}$).
- Surfaces expose a variety of potential binding sites of different coordination numbers.
- Real surfaces will always have a number of defects (steps, kinks, missing atoms, etc.).
- Clean surfaces can exhibit either relaxations or reconstructions.
- Relaxations are slight changes in bond lengths and angles.
- Reconstructions are changes in the periodicity of the surface compared with the bulk-terminated structure.
- Adsorbates can form ordered or random structures and may either distribute themselves homogeneously over the surface or in islands.
- Adsorbates can also lead to changes in the surface structure of the substrate inducing either a lifting of the clean surface reconstruction or the formation of an entirely new surface reconstruction.

- The occupation of electronic states is defined by the Fermi-Dirac distribution (Equation 1.3.5).
- Surface electronic states exist in a bulk bandgap.
- A surface resonance has a wavefunction that is concentrated at the surface but it does not exist in a bandgap and, therefore, interacts strongly with bulk states.
- Vibrations in solids are quantized and form bands analogous to the band structure of electronic states.
- The mean phonon occupation number follows the Planck distribution law (Equation 1.4.7).
- Properties of matter become size dependent as the contributions of surface atoms start to outweigh those bulk atoms and as quantum confinement effects set in.
- Both the electronic structure and the phonon spectrum change as particle size approaches the nanoscale.

1.6 Frontiers and Challenges

- Excited electronic states. As we will see in the chapter on stimulated (nonthermal) chemistry, excited states play a central role and their description at surfaces is fraught.
- Producing porous materials with controlled composition, pore size and pore morphology.
- The surface science of chirality.
- Characterization and explanation of the electronic, optical, geometric, magnetic and chemical properties of nanoscale features on surfaces.
- Characterization and description of defects on solid surfaces.
- The relationship between surface structure, bulk reduction and surface reactivity of oxide surfaces.

1.7 Further Reading

S. Elliott, *The Physics and Chemistry of Solids*, John Wiley & Sons, Ltd, Chichester (1998).
C. Kittel, *Introduction to Solid State Physics*, John Wiley & Sons, Ltd, New York (1986).
Walter A. Harrison, *Solid State Theory*, Dover Publications, Inc., New York (1979).
H. Lüth, *Surfaces and Interfaces of Solid Materials*, Springer-Verlag, Berlin (1995).
S. Roy Morrison, *Electrochemistry at Semiconductor and Oxidized Metal Electrodes*, Plenum, New York (1980).
Herbert Over, 'Crystallographic study of interaction between adspecies on metal surfaces', *Prog. Surf. Sci.* **58** (1998) 249.
M.W. Roberts, C.S. McKee, *Chemistry of the Metal–Gas Interface*, Clarendon Press, Oxford (1978).
G.A. Somorjai, *Introduction to Surface Chemistry and Catalysis*, John Wiley & Sons, Ltd, New York (1994).
S.M. Sze, *Physics of Semiconductor Devices*, John Wiley & Sons, Ltd, New York (1981).
S. Titmuss, A. Wander D.A. King, 'Reconstruction of clean and adsorbate-covered metal surfaces', *Chem. Rev.* **96**, (1996) 1291.
A. Zangwill, *Physics at Surfaces*, Cambridge University Press, Cambridge (1988).

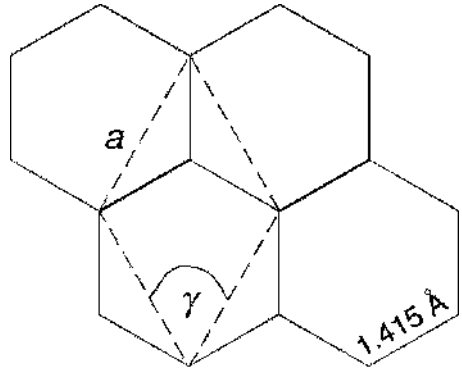

Figure 1.20 *A schematic drawing of the structure of the basal plane of graphite.*

1.8 Exercises

1.1 For the basal (cleavage) plane of graphite, determine the surface unit cell length, a, the included angle between sides of the unit cell, γ, and the density of surface C atoms, σ_0, given that the C–C nearest neighbour distance is 1.415 Å. A representation of the graphite surface is given in Figure 1.20.

1.2 The Fermi energies of Cs, Ag and Al are 1.59, 5.49 and 11.7 eV, respectively.[53] Calculate the density of the Fermi electron gas in each of these metals as well as the Fermi temperature. Calculate the difference between the chemical potential and the Fermi energy for each of these metals at their respective melting points.

1.3 A clean Ag(111) surface has a work function of 4.7 eV. As a submonolayer coverage of Ba is dosed onto the surface, the work function drops and reaches a minimum of 2.35 eV.[68] Calculate the surface potential associated with the clean and Ba covered surfaces and explain the effect of Ba adsorption on the work function of Ag(111).

1.4 The work function of clean Al(111) is 4.24 eV[69] (a free electron *sp* metal), clean Ag (111) is 4.7 eV[68] (a coinage metal) and for bulk polycrystalline Cs is 2.14 eV (an alkali metal). Use the value of the Fermi energy given in Exercise 1.1 to calculate the surface potential for these three different types of metals.

1.5 The magnitude of an electric dipole μ is

$$\mu = qR \tag{1.8.1}$$

for a charges $+q$ and $-q$ separated by a distance R. The work function change $\Delta\Phi$ expressed in eV associated with adsorption of a species with charge q, located a distance $R/2$ from the surface (hence its image charge is at a distance R from the adsorbate and $-R/2$ below the plane of the surface) at a coverage σ is given by the *Helmholtz equation*

$$\Delta\Phi = 2\pi\sigma\mu, \tag{1.8.2}$$

when the dipole moment μ is expressed in debye ($1\text{D} = 3.33564 \times 10^{-30}\,\text{C m}$).

Calculate the work function changes expected for peroxo (O_2^{2-}) and superoxo (O_2^-) species bound on Pd(111) given that their bond distance is 2 Å. The measured work function change is only on the order of 1 eV. Explain the difference between your estimates and the measured value.

1.6 The work function of Pt(111) is 5.93 eV. A Ru film has a work function of 4.71 eV. If Ru islands are deposited on a Pt(111) surface, in which direction does electron transfer occur?

1.7 Redraw Figure 1.13 for a *p*-type semiconductor.[53,55]

1.8 Given that the *partition function*, q, is defined by a summation over all states according to

$$q = \sum_{i=1}^{\infty} \exp(-E_i/k_B T) \tag{1.8.3}$$

where E_i is the energy of the ith state, use Equation (1.4.4) to show that the mean vibrational energy of a solid at equilibrium is given by Equation (1.4.6).

Hint: The mean energy is given by

$$\langle E \rangle = k_B T^2 \frac{\partial(\ln q)}{\partial T} \tag{1.8.4}$$

1.9 The *Debye temperature* is given by

$$\theta_D = \frac{\hbar \omega_D}{k_B} \tag{1.8.5}$$

and is more commonly tabulated and determined than is the *Debye frequency* because of its relationship to the thermodynamic properties of solids.

(a) Calculate the Debye frequencies of the elemental solids listed in Table 1.1 in Hz, meV and cm^{-1}.

(b) Calculate the mean phonon occupation number at the Debye frequency and room temperature for each of these materials at 100, 300 and 1000 K.

1.10 The *Debye model* (see Table 1.3) can be used to calculate the mean square displacement of an oscillator in a solid. In the high-temperature limit this is given by

$$\langle u^2 \rangle = \frac{3N_A \hbar^2 T}{M k_B \theta_D^2} \tag{1.8.6}$$

(a) Compare the root-mean-square displacements of Pt at 300 K to that at its melting point (2045 K). What is the fractional displacement of the metal atoms relative to the interatomic distance at the melting temperature?

(b) Compare this with the root-mean-square displacement of the C atoms at the surface of diamond at the same two temperatures.

Table 1.3 *Debye temperatures, θ_D, for selected elements; see Exercises 1.4 and 1.5.*

	Ag	Au	diamond	graphite	Pt	Si	W
θ_D (K)	225	165	2230	760	240	645	400

1.11 The *surface Debye temperature* of Pt(100) is 110 K. Take the definition of melting to be when the fractional displacement relative to the lattice constant is equal to ~8.3 % (*Lindemann criterion*.[70,71]) What is the *surface melting* temperature of Pt (100)? What is the implication of a surface that melts at a lower temperature than the bulk?

1.12 The bulk terminated Si(100)–(1×1) surface has two dangling bonds per surface atom and is, therefore, unstable toward reconstruction. Approximate the dangling bonds as effectively being half-filled sp^3 orbitals. The driving force of reconstruction is the removal of dangling bonds.

(a) The stable room temperature surface reconstructs into a (2×1) unit cell in which the surface atoms move closer to each other in one direction but the distance is not changed in the perpendicular direction. Discuss how the loss of one dangling bond on each Si atom leads to the formation of a (2×1) unit cell. Hint: The nearest neighbour surface Si atoms are called dimers.

(b) This leaves one dangling bond per surface atom. Describe the nature of the interaction of these dangling bonds that leads to (1) symmetric dimers and (2) tilted dimers.

(c) Predict the effect of hydrogen adsorption on the symmetry of these two types of dimers.[40,41] Hint: Consider first the types of bonds that sp^3 orbitals can make. Second, two equivalent dangling bonds represent two degenerate electronic states.

1.13 (a) Derive a general expression for the *step density*, ρ_{step}, of an fcc crystal with single-atom-height steps induced by a miscut angle χ from the ideal surface plane.

(b) Make a plot of step density versus miscut angle for the Pt(111) surface, which has a surface atom density of $\sigma_0 = 1.503 \times 10^{15}\,\mathrm{cm}^{-2}$.

References

1. J. F. Nicholas, *An Atlas of Models of Crystal Structures*, Gordon and Breach, New York, (1961).
2. M. W. Roberts, C. S. McKee, *Chemistry of the Metal–Gas Interface*, Clarendon Press, Oxford (1978).
3. H.-J. Gossmann, L. C. Feldman, *Phys. Rev. B*, **32** (1985) 6.
4. H.-C. Jeong, E. D. Williams, *Surf. Sci. Rep.*, **34** (1999) 171.
5. R. Smoluchowski, *Phys. Rev.*, **60** (1941) 661.
6. V. A. Shchukin, D. Bimberg, *Rev. Mod. Phys.*, **71** (1999) 1125.
7. R. M. Watwe, R. D. Cortright, M. Mavirakis, J. K. Nørskov, J. A. Dumesic, *J. Chem. Phys.*, **114** (2001) 4663.
8. C. T. Campbell, *Annu. Rev. Phys. Chem.*, **41** (1990) 775.
9. J. J. Steele, M. J. Brett, *J. Mater. Sci.*, **18** (2007) 367.
10. A. G. Cullis, L. T. Canham, P. D. J. Calcott, *J. Appl. Phys.*, **82** (1997) 909.
11. S. Langa, J. Carstensen, M. Christophersen, K. Steen, S. Frey, I. M. Tiginyanu, H. Föll, *J. Electrochem. Soc.*, **152** (2005) C525.
12. I. V. Sieber, P. Schmuki, *J. Electrochem. Soc.*, **152** (2005) C639.
13. R. Beranek, H. Hildebrand, P. Schmuki, *Electrochem. Solid State Lett.*, **6** (2003) B12.
14. H. Tsuchiya, J. M. Macak, I. Sieber, L. Taveira, A. Ghicov, K. Sirotna, P. Schmuki, *Electrochem. Commun.*, **7** (2005) 295.
15. H. Tsuchiya, J. M. Macak, L. Taveira, P. Schmuki, *Chem. Phys. Lett.*, **410** (2005) 188.

16. H. Masuda, K. Fukuda, *Science*, **268** (1995) 1466.
17. X. He, D. Antonelli, *Angew. Chem.*, Int. Ed. Engl., **41** (2002) 214.
18. M. A. Carreon, V. V. Guliants, *Eur. J. Inorg. Chem.*, **2005** (2005) 27.
19. G. S. Armatas, M. G. Kanatzidis, *Science*, **313** (2006) 817.
20. G. W. Nyce, J. R. Hayes, A. V. Hamza, J. H. Satcher, Jr., *J. Phys. Chem. C* **19** (2007) 344.
21. O. D. Velev, A. M. Lenhoff, *Curr. Opin. Colloids Interface Sci.*, **5** (2000) 56.
22. R. B. Wehrspohn, H. S. Kitzerow, *Phys. J.*, **4** (2005) 35.
23. M. Ulbricht, *Polymer*, **47** (2006) 2217.
24. C. Dekker, *Nature Nanotech.*, **2** (2007) 209.
25. J. M. Thomas, W. J. Thomas, *Principles and Practice of Heterogeneous Catalysis*, VCH, Weinheim (1996).
26. N. W. Ockwig, O. Delgado-Friedrichs, M. O'Keeffe, O. M. Yaghi, *Acc. Chem. Res.*, **38** (2005) 176.
27. J. L. C. Rowsell, O. M. Yaghi, *Microporous Mesoporous Mater.*, **73** (2004) 3.
28. J. L. C. Rowsell, O. M. Yaghi, *Angew. Chem., Int. Ed. Engl.*, **44** (2005) 4670.
29. A. P. Cote, A. I. Benin, N. W. Ockwig, M. O'Keeffe, A. J. Matzger, O. M. Yaghi, *Science*, **310** (2005) 1166.
30. D. P. Woodruff (Ed.), *The Chemical Physics of Solid Surfaces and Heterogeneous Catalysis: Oxide Surfaces*, *Vol. 9*, Elsevier, Amsterdam, (2001).
31. K. Sohlberg, S. J. Pennycook, S. T. Pantelides, *J. Am. Chem. Soc.*, **121** (1999) 7493.
32. P. W. Tasker, *J. Phys. C*, **12** (1979) 4977.
33. H. J. Freund, *Faraday Discuss.*, **114** (1999) 1.
34. U. Diebold, *Surf. Sci. Rep.*, **48** (2003) 53.
35. M. Bowker, *Curr. Opin. Solid State Mater. Sci.*, **10** (2006) 153.
36. A. Patrykiejew, S. Sokolowski, K. Binder, *Surf. Sci. Rep.*, **37** (2000) 207.
37. G. A. Somorjai, *Introduction to Surface Chemistry and Catalysis*, John Wiley & Sons, Ltd, New York (1994).
38. G. A. Somorjai, *Ann. Rev. Phys. Chem.*, **45** (1994) 721.
39. G. Ertl, *Langmuir*, **3** (1987) 4.
40. K. W. Kolasinski, *Internat. J. Mod. Phys. B*, **9** (1995) 2753.
41. R. Becker, R. Wolkow, Semiconductor Surfaces: Silicon in *Scanning Tunneling microscopy* (Eds. J. A. Stroscio, W. J. Kaiser), Academic Press, Boston (1993) 149.
42. Y. J. Chabal, K. Raghavachari, *Phys. Rev. Lett.*, **54** (1985) 1055.
43. J. J. Boland, *Adv. Phys.*, **42** (1993) 129.
44. J. E. Northrup, *Phys. Rev. B*, **44** (1991) 1419.
45. R. Imbihl, G. Ertl, *Chem. Rev.*, **95** (1995) 697.
46. B. Kesanli, W. B. Lin, *Coord. Chem. Rev.*, **246** (2003) 305.
47. L. A. DeLouise, B. L. Miller, *Anal. Chem.*, **76** (2004) 6915.
48. C. F. McFadden, P. S. Cremer, A. J. Gellman, *Langmuir*, **12** (1996) 2483.
49. G. A. Attard, A. Ahmadi, J. Feliu, A. Rodes, E. Herrero, S. Blais, G. Jerkiewicz, *J. Phys. Chem. B*, **103** (1999) 1381.
50. T. Greber, Z. Sljivancanin, R. Schillinger, J. Wider, B. Hammer, *Phys. Rev. Lett.*, **96** (2006) 056103.
51. S. J. Pratt, S. J. Jenkins, D. A. King, *Surf. Sci.*, **585** (2005) L159.
52. K. Besocke, B. Krahl-Urban, H. Wagner, *Surf. Sci.*, **68** (1977) 39.
53. S. Elliott, *The Physics and Chemistry of Solids*, John Wiley & Sons, Ltd, Chichester (1998).
54. S. M. Sze, *Physics of Semiconductor Devices*, 2nd ed., John Wiley & Sons, Ltd, New York (1981).
55. S. R. Morrison, *Electrochemistry at Semiconductor and Oxidized Metal Electrodes*, Plenum, New York (1980).
56. H. Gerischer, *Electrochim. Acta*, **35** (1990) 1677.
57. H. Lüth, *Surfaces and Interfaces of Solid Materials*, 3rd ed, Springer-Verlag, Berlin, (1995).
58. N. J. Halas, J. Bokor, *Phys. Rev. Lett.*, **62** (1989) 1679.
59. R. Haight, *Surf. Sci. Rep.*, **21** (1995) 275.
60. W. Steinmann, T. Fauster, Two-Photon Photoelectron Spectroscopy of Electronic States at Metal Surfaces, in *Laser Spectroscopy and Photochemistry on Metal Surfaces. Part I* (Eds. H.-L. Dai, W. Ho), World Scientific, Singapore (1995) 184.

61. U. Höfer, I. L. Shumay, C. Reuß, U. Thomann, W. Wallauer, T. Fauster, *Science*, **277** (1997) 1480.
62. M. Wolf, E. Knoesel, T. Hertel, *Phys. Rev. B*, **54** (1996) 5295.
63. H. Richter, Z. P. Wang, L. Ley, *Solid State Commun.*, **39** (1981) 625.
64. I. H. Campbell, P. M. Fauchet, *Solid State Commun.*, **58** (1986) 739.
65. S. P. Hepplestone, G. P. Srivastava, *Nanotechnology*, **17** (2006) 3288.
66. M. A. Stroscio, M. Dutta, *Phonons in Nanostructures*, Cambridge University Press, Cambridge, (2001).
67. M. N. Islam, S. Kumar, *Appl. Phys. Lett.*, **78** (2001) 715.
68. O. M. N. D. Teodoro, J. Los, A. M. C. Moutinho, *J. Vac. Sci. Technol. A*, **20** (2002) 1379.
69. A. Hohlfeld, M. Sunjic, K. Horn, *J. Vac. Sci. Technol. A*, **5** (1987) 679.
70. J. J. Gilvarry, *Phys. Rev.*, **102** (1956) 308.
71. F. A. Lindemann, *Phys. Z.*, **11** (1910) 609.